



universität
wien

MASTERARBEIT

Titel der Masterarbeit

„Pulsed Quantum Optomechanics“

verfasst von

Joachim Hofer, BSc

angestrebter akademischer Grad

Master of Science (MSc)

Wien, 2015

Studienkennzahl lt. Studienblatt:

A 066 876

Studienrichtung lt. Studienblatt:

Physik

Betreut von:

Univ.-Prof. Dr. Markus Aspelmeyer

Abstract

Quantum optomechanics is one of the most promising approaches to study the quantum behaviour of macroscopic objects and do experimental quantum mechanics in a new regime (of large mass as well as large size). This allows us to experimentally probe quantum decoherence theories and might even provide a route to experimental tests of theories of quantum gravity.

While most of the early attention in this field has gone to the interaction of a continuous field (in a cavity) with a mechanical resonator, recently other configurations have been considered as well. In particular, the use of short optical pulses shows great promise to overcome the limits inherent to the continuous scheme by avoiding any back-action on the position of the mirror and to thereby perform a quantum-non-demolition measurement of the mechanical position.

In this thesis we construct a proof-of-concept setup using short optical pulses to perform a quantum-non-demolition measurement of the position of a mechanical resonator. We demonstrate the preparation of squashed thermal states with a position uncertainty of down to 19pm (reduced from an initial uncertainty of 1.2nm) limited only by the optical quantum noise of the pulses. We furthermore perform a full tomography of these mechanical states and reconstruct the Wigner function.

Future enhancements to our setup will allow for the preparation of mechanical quantum states even at room temperature. Also, as our tomographic scheme is not subjected to the standard quantum limit, it is possible to perform tomography on mechanical quantum states containing features smaller than the ground state.

Zusammenfassung

Quanten-Optomechanik erlaubt es, quantenmechanische Eigenschaften von makroskopischen Objekten zu untersuchen und etabliert experimentelle Quantenmechanik in einem neuen Regime (sowohl bzgl. Masse als auch Größe). Dies ermöglicht experimentelle Tests von Dekohärenz-Theorien und in naher Zukunft möglicherweise sogar von Theorien zur Quantengravitation.

Anfangs wurde hauptsächlich die Wechselwirkung zwischen kontinuierlichen optischen Feldern und einem mechanischen Resonator untersucht, in den letzten Jahren wurden aber auch viele alternative Ansätze in Erwägung gezogen. Vor allem die Verwendung kurzer optischer Pulse statt eines kontinuierlichen Feldes muss hier erwähnt werden, da bei diesem Ansatz die mechanische Position während der Wechselwirkung nicht verändert wird, was eine zerstörungsfreie Quantenmessung (quantum-non-demolition measurement) der mechanischen Position ermöglicht.

In Verlauf dieser Masterarbeit errichteten wir ein Setup, welches als Nachweis der Machbarkeit einer solchen gepulsten Messung dienen soll. Wir zeigen die Vorbereitung mechanischer Zustände mit einer reduzierten Orts-Unsicherheit von 19pm (ausgehend von 1.2nm im thermischen Anfangszustand), welche lediglich durch das Schrotrauschen der verwendeten optischen Pulse limitiert ist. Weiters implementieren wir einen tomographischen Algorithmus, welcher die Rekonstruktion der Wignerfunktion des mechanischen Zustands ermöglicht.

Zukünftige Verbesserungen an unserem Setup werden die Vorbereitung quantenmechanischer Zustände bei Raumtemperatur ermöglichen. Zusätzlich erlaubt uns unsere tomographische Messmethode die Rekonstruktion quantenmechanischer Zustände, selbst wenn die ursprüngliche Wahrscheinlichkeitsverteilung Merkmale auf einer Längenskala gegeben durch den Grundzustand enthält.

Contents

1	Optomechanics	3
1.1	Harmonic oscillators	3
1.1.1	Classical description	3
1.1.2	Quantum mechanical description	8
1.2	Classical description of optomechanical systems	11
1.2.1	The electromagnetic field	11
1.2.2	Optical cavities	13
1.2.3	Optomechanics	16
1.3	Quantum mechanical description of optomechanical systems	19
1.3.1	Quantum electrodynamics	19
1.3.2	Quantum optomechanics	20
2	Quantum measurements and quantum state tomography	23
2.1	Quantum tomography	24
2.1.1	The Wigner function	25
2.1.2	Reconstruction of the Wigner function	26
2.2	Quantum measurement	27
2.2.1	Quantum measurement theory	28
2.2.2	Indirect measurements	31
3	Experimental techniques	33
3.1	Lasers and electromagnetic beams	33
3.2	Interferometry	34
3.3	The beam splitter	34
3.4	Photodetectors	36
3.5	Homodyne detection	38
3.6	Mechanical oscillators and the effective mass	41
4	Pulsed quantum optomechanics	44
4.1	Theory	44
4.1.1	General	45
4.1.2	State preparation	46
4.1.3	State reconstruction	50
4.2	Proof-of-concept Experiment	50
4.2.1	Setup	50
4.2.2	Measurement	52
4.2.3	The mechanical oscillator	52
4.2.4	Calibration	53
4.2.5	Verification of the shot noise limit	53
4.2.6	Coupling to a thermal environment	54
4.3	Results	54
5	Discussion & Outlook	57
A	Pulsed cavity optomechanics	61
	Curriculum vitae (german)	63

Introduction

Ever since the early days of quantum mechanics physicists have tried to establish a correspondence between the classical world and the quantum world. While there has been a tremendous progress in the last century and many of the interpretational problems (like the measurement problem) can now qualitatively (and often also quantitatively) be explained by quantum decoherence, there still exists no universally accepted theory and many open questions remain.

To study these questions experimentally one has to be able to both prepare macroscopic objects in quantum states and to characterize the time-evolution of these states. The last years have shown tremendous progress towards the preparation of such states using cavity-optomechanics leading to the preparation of macroscopic mechanical oscillators into their quantum ground state [1][2][3]. In addition, entanglement between microwave fields and the motion of a mechanical resonator has been demonstrated [4].

However, as these techniques are typically based on continuous interaction of a stationary coherent optical state with the mechanical resonator and therefore subjected to the standard quantum limit (SQL), it is generally not possible to prepare and/or measure mechanical features smaller than the ground state.

An elegant solution to this problem is pulsed quantum optomechanics [5], which utilizes short optical pulses to perform a quantum-non-demolition (QND) measurement of the mechanical position. Due to the QND character of the measurement, it is in principle possible to achieve measurement accuracies below the SQL and leave the mechanical oscillator in a state with squeezed position quadrature. As this squeezing-by-measurement can be done on a hitherto unreachable timescale only limited by the pulse duration, it significantly relaxes the requirements on shielding the system from the environment.

Furthermore, the pulsed scheme can be used to perform quantum tomography of mechanical states with an accuracy below the SQL. This allows for a complete characterization of the mechanical state (even for mechanical quantum states described by a Wigner distribution that takes on negative values) and, in particular, it provides a way to study decoherence mechanisms.

The purpose of this thesis is the description of a proof-of-concept experiment implementing pulsed optomechanics as described in [5] and to summarize the obtained results. In the first two sections I am going to introduce the basic theory necessary to understand the experiment. I am going to assume some familiarity with classical and quantum mechanics, but the aim was that this thesis can be read and understood by an advanced undergraduate student. The first two sections might also serve on their own as an introduction in quantum optomechanics and quantum measurement theory. The third section concerns itself with more technical aspects and connects the theory of the first two chapters to the implementation of a typical quantum-optomechanics experiment. Finally, in the fourth section, I am going to apply the theory of section 1 & 2 to our experiment, introduce the setup and describe the results. The fifth and last section provides a short discussion of the results and outlines possible future improvements and applications.

1 Optomechanics

As the name implies, optomechanics is the study of the interaction between optical systems (i.e. electromagnetic radiation) and (macroscopic) mechanical systems. One of the main mechanisms by which such systems interact is radiation pressure, i.e. the pressure exerted on surfaces by incident radiation, which can be due to the reflection of the radiation or the absorption (or a combination of both). In most cases the optical field is generated by a (single mode) laser and the mechanical system consists of a highly reflective mechanical oscillator. In this chapter we derive the formalism to describe such optomechanical systems, both classically and quantum mechanically. Since the harmonic oscillator plays an important role in the description of mechanical oscillators as well as optical systems, the first section of this chapter is dedicated to provide a quick (but thorough) introduction in its theory.

1.1 Harmonic oscillators

1.1.1 Classical description

A classical (one-dimensional) harmonic oscillator is a system which is described by the differential equation

$$\ddot{x} + \omega^2 x = 0, \tag{1}$$

where x is some observable (i.e. measurable quantity) of the system and ω is a constant. Typical examples for (approximately) harmonic oscillators include (in the absence of dissipation) mechanical harmonic oscillators and LC circuits (the observables are the mechanical position and the charge, respectively). The general solution of this differential equation is given by

$$x(t) = x(0) \cos(\omega t) + \frac{\dot{x}(0)}{\omega} \sin(\omega t).$$

We will from now on focus on the case of an ideal mechanical system, where x describes the position of a test mass m . We can define the spring constant k through $\omega = \sqrt{\frac{k}{m}}$, this leads to the equation

$$m\ddot{x} = -kx,$$

which is often used instead of equation 1 as the starting point in the investigation of mechanical harmonic oscillators.

The energy of such a system is conserved and given by

$$E = \frac{p^2}{2m} + \frac{m\omega^2 x^2}{2},$$

where we have introduced the momentum $p = m\dot{x}$.

A more experimentally relevant system is given by the damped harmonic oscillator, which is described by the equation

$$\ddot{x} + \gamma\dot{x} + \omega^2 x = 0$$

and provides a realistic model for mechanical harmonic oscillators, if the dominating cause of dissipation is linear drag. The solution of this differential equation depends on the sign of $\gamma - 2\omega$ and one therefore has to distinguish between three cases:

- (i) $\gamma < 2\omega$: $x(t) = e^{-\frac{\gamma}{2}t} \left[x(0) \cos(\Omega t) + \frac{\dot{x}(0) + \frac{\gamma}{2}x(0)}{\Omega} \sin(\Omega t) \right]$.
- (ii) $\gamma = 2\omega$: $x(t) = e^{-\frac{\gamma}{2}t} \left[x(0) \cosh(\Omega t) + \frac{\dot{x}(0) + \frac{\gamma}{2}x(0)}{\Omega} \sinh(\Omega t) \right]$.
- (iii) $\gamma > 2\omega$: $x(t) = e^{-\frac{\gamma}{2}t} \left[x(0) + \left(\dot{x}(0) + \frac{\gamma}{2}x(0) \right) t \right]$.

If the dissipation is small ($\gamma < 2\omega$), one still observes oscillations with a decreasing amplitude and shifted frequency

$$\Omega = \sqrt{|\omega^2 - \frac{\gamma^2}{4}|}$$

compared to the ideal harmonic oscillator (i.e. $\gamma = 0$). On the other hand, if $\gamma \geq 2\omega$, there the oscillatory behaviour of the system vanishes. The behaviour of the solutions in each of the cases can be seen in figure 1. It is interesting to note that (for fixed ω) the fastest decay can be observed for case (ii), i.e. if $\gamma = 2\omega$ (critical damping).

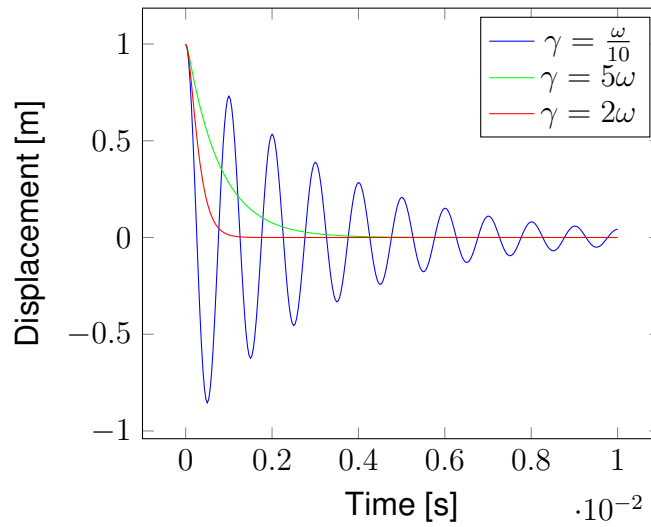


Figure 1: Behaviour of a damped harmonic oscillator for $x(0) = 1m$, $\dot{x}(0) = 0 \frac{m}{s}$, $m = 1kg$, $\omega = 2\pi \cdot 1kHz$ and different damping strengths.

An important parameter of a damped harmonic oscillator is its quality factor, which is defined by

$$Q = \frac{\omega}{\gamma}.$$

If $Q \gg \frac{1}{2}$ (i.e. a strongly oscillating system), it makes sense to define the energy of the damped harmonic oscillator as

$$E(t) = \frac{m}{2} (\omega^2 x^2(t) + \dot{x}^2(t)),$$

and it follows, that

$$Q \approx 2\pi \frac{E(0)}{E(T) - E(0)}$$

or more generally, $\frac{Q}{2\pi}$ approximates the ratio of the stored energy to the energy lost in the next period.

One can also investigate the behaviour of a harmonic system under the effect of some force, the associated differential equation is

$$\ddot{x} + \gamma\dot{x} + \Omega^2 x = \frac{F}{m}, \quad (2)$$

where F now stands for the external force acting on the oscillator (note the slight change in notation, since ω will be used as a variable in the frequency domain). Such a system is sometimes called a damped and driven harmonic oscillator and can even be used to describe the thermal motion of mechanical harmonic oscillators. In general, this differential equation cannot be solved analytically. We will quickly investigate the simple case of a harmonic driving force, for which a analytic solution exists, and then provide a more general framework for dealing with equation 2 based on frequency analysis.

Assume for now that

$$F(t) = \text{Re} \left[A(\omega) e^{-i\omega t} \right]$$

and choose the ansatz $x_p(t) = \text{Re} \left[B(\omega) e^{-i\omega t} \right]$ for the particular solution. The reason for writing down the complex expressions is solely calculational simplicity, physical equations can be obtained at any time by taking the real part of the expressions. Note that, while $A(\omega)$ is chosen to be real, $B(\omega) = |B(\omega)| e^{i\phi(\omega)}$ has to be complex to include a shift in the phase of the oscillator (relative to the driving force). This ansatz leads to

$$B(\omega) = \frac{A(\omega)}{m(\Omega^2 - \omega^2 - i\gamma\omega)} = \chi(\omega) A(\omega),$$

where we have defined the mechanical susceptibility

$$\chi(\omega) = \frac{1}{m(\Omega^2 - \omega^2 - i\gamma\omega)}.$$

The amplitude and phase response are given by

$$|B(\omega)| = |\chi(\omega)| A(\omega)$$

and

$$\phi(\omega) = \arctan \left(\frac{\text{Im}[\chi(\omega)]}{\text{Re}[\chi(\omega)]} \right)$$

and plotted in figure 2.

The solution of the differential equation can now be obtained by the sum of the homogeneous solution and the particular solution $x_p(t)$. After the initial ring-down only the particular solution remains.

In the frequency domain, (assuming the Fourier transform of F exists at all), equation 2 reads

$$x(\omega) = \chi(\omega) F(\omega) \quad (3)$$

with the Fourier transform defined by

$$f(\omega) = \int_{-\infty}^{\infty} dt f(t) e^{i\omega t}$$

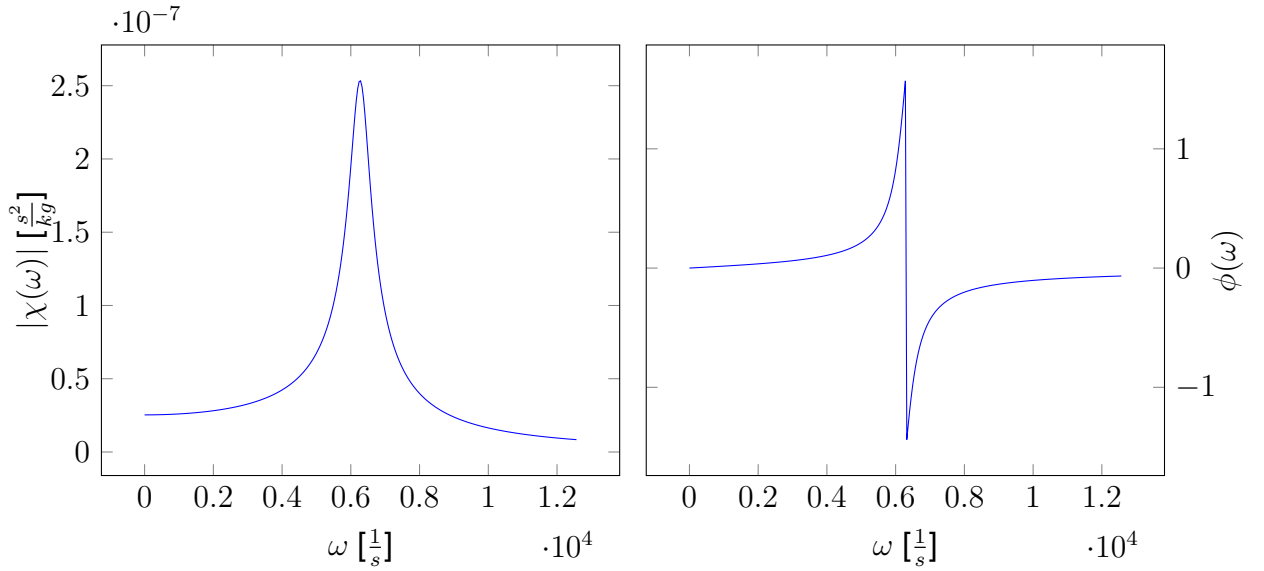


Figure 2: Typical amplitude and phase response of a driven, damped harmonic oscillator ($\Omega = 2\pi \cdot 1kHz$, $\gamma = \frac{\omega}{10}$, $m = 1kg$).

and $\chi(\omega)$ defined as above (note that commonly used definitions of the susceptibility may differ in the sign of the imaginary part - this is simply due to a different definition of the Fourier transform). The particular solution in the time-domain can then be expressed as

$$x_p(t) = \frac{1}{2\pi} \int_{-\infty}^{\infty} d\omega \chi(\omega) F(\omega) e^{-i\omega t}.$$

Using the convolution theorem we can express this as

$$x_p(t) = \int_{-\infty}^{\infty} dt' \chi(t - t') F(t),$$

where $\chi(t)$ is of course the inverse Fourier transform of $\chi(\omega)$, i.e.

$$\chi(t) = \frac{1}{2\pi} \int_{-\infty}^{\infty} d\omega \chi(\omega) e^{-i\omega t}.$$

This expression exists and can be evaluated analytically (see e.g. [18]), in particular one finds that $\chi(t - t') = 0$ for $t' > t$, i.e. the response of the system is causal.

The work done by the external force (i.e. the energy dissipated) is given by

$$\Delta E = \int_{-\infty}^{\infty} dt F(t) \dot{x}(t).$$

Expressing this with the respective Fourier transforms and using $F(-\omega) = F(\omega)^*$ (i.e. taking $F(t)$ as real) as well as $\int_{-\infty}^{\infty} dt e^{i(\omega - \omega')t} = 2\pi\delta(\omega - \omega')$ we arrive at

$$\Delta E = -\frac{i}{2\pi} \int_{-\infty}^{\infty} d\omega \omega \chi(\omega) |F(\omega)|^2 = -\frac{i}{2\pi} \int_{-\infty}^{\infty} d\omega \frac{\omega}{\chi(\omega)^*} |x(\omega)|^2.$$

Since the real part of the susceptibility fulfills $Re[\chi(\omega)] = Re[\chi(-\omega)]$, this expression depends only on the imaginary part of χ :

$$\Delta E = -\frac{i}{2\pi} \int_{-\infty}^{\infty} d\omega \omega Im[\chi(\omega)] |F(\omega)|^2 = \frac{i\gamma}{2\pi} \int_{-\infty}^{\infty} d\omega \omega^2 |x(\omega)|^2.$$

Note that in general the expression for the work doesn't converge (a finite force acting for an infinite amount of time obviously leads to an infinite amount of work) and therefore one often considers the power rather than the energy.

We start by defining the windowed Fourier transform

$$x_T(\omega) := \frac{1}{\sqrt{2T}} \int_{-T}^T dt x(t) e^{i\omega t}$$

and notice, that

$$\frac{1}{2\pi} \int_{-\infty}^{\infty} d\omega |x_T(\omega)|^2 = \frac{1}{2T} \int_{-T}^T dt x(t)^2.$$

This allows us to connect the power spectral density

$$S_{xx}(\omega) := \lim_{T \rightarrow \infty} |x_T(\omega)|^2$$

to the variance

$$\langle x(t)^2 \rangle := \lim_{T \rightarrow \infty} \frac{1}{2T} \int_{-T}^T dt x(t)^2$$

by

$$\int_{-\infty}^{\infty} d\omega S_{xx}(\omega) = 2\pi \langle x(t)^2 \rangle.$$

An important application is the thermal force (i.e. the force acting on a harmonic oscillator in thermal equilibrium), for which the equipartition theorem connects the variance to the temperature by

$$\langle x(t)^2 \rangle = \frac{k_B T}{m\Omega^2}. \quad (4)$$

Defining $F_T(\omega)$ in analogy to $x_T(\omega)$, we furthermore get

$$\langle x(t)^2 \rangle = \frac{1}{2\pi} \int_{-\infty}^{\infty} d\omega |\chi(\omega)|^2 \lim_{T \rightarrow \infty} |F_T(\omega)|^2.$$

Because thermal noise is white (i.e. independent of ω), we can solve for the force power spectral density $\lim_{T \rightarrow \infty} |F_T(\omega)|^2$ and, evaluating the integral and using the equipartition theorem, this leads to

$$\lim_{T \rightarrow \infty} |F_T(\omega)|^2 = 2k_B T m \gamma.$$

and

$$S_{xx}(\omega) = 2k_B T m \gamma |\chi(\omega)|^2.$$

Note that this can be expressed as

$$S_{xx}(\omega) = \frac{2k_B T}{\omega} \text{Im}[\chi(\omega)],$$

which is a commonly used form of the fluctuation-dissipation theorem.

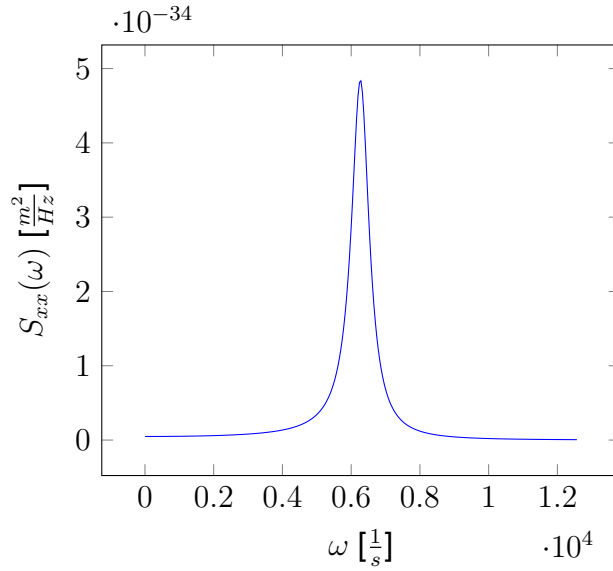


Figure 3: Power spectral density of a harmonic oscillator (same properties as in figure 2) at room temperature (273K).

1.1.2 Quantum mechanical description

Since a rigorous introduction to quantum mechanics is outside the scope of this thesis, I will assume that the reader is already familiar with it (and, in particular, the Dirac notation). We will follow the canonical way to pass from classical mechanics to quantum mechanics. The energy of an ideal harmonic oscillator is given by equation 2. We replace the position x and the momentum p by the corresponding operators and get the Hamilton operator of a harmonic oscillator

$$H = \frac{P^2}{2m} + \frac{m\omega^2 X^2}{2}, \quad (5)$$

where operators are denoted by capital letters (with the exception of the creation/annihilation operators a and a^\dagger defined below). The operators X and P obey the commutation relation

$$[X, P] = i\hbar \mathbb{1}.$$

One could now solve the (stationary) Schroedinger equation in a particular representation, e.g. (note that E denotes the energy of the system and is a scalar, not an operator)

$$E\psi(x) = \left(-\frac{1}{2m} \frac{\partial^2}{\partial x^2} + \frac{m\omega^2 x^2}{2} \right) \psi(x), \quad (6)$$

to obtain the states of the system (and all other quantities of interest). We will however take the algebraic approach, i.e. instead of solving a second-order differential equation we will treat the Schroedinger equation as an eigenvalue problem in the Hilbert space,

$$H|\psi\rangle = E|\psi\rangle, \quad (7)$$

and use (almost) purely algebraic methods to find the eigenvalues and the corresponding eigenstates.

Using natural units, i.e. introducing "new" position and momentum operators as

$$X_0 = \sqrt{\frac{m\omega}{2\hbar}} X \quad \text{and} \quad P_0 = \sqrt{\frac{1}{2m\hbar\omega}} P,$$

the annihilation operator is now defined by

$$a = X_0 + iP_0$$

and the creation operator is its adjunct and defined by

$$a^\dagger = X_0 - iP_0.$$

From these definitions and the commutation relations of X_0 and P_0 ,

$$[X, P] = i\hbar\mathbb{1} \implies [X_0, P_0] = i\frac{1}{2}\mathbb{1},$$

we obtain the commutation relation for a and a^\dagger :

$$[a, a^\dagger] = \mathbb{1}.$$

The Hamilton operator can now easily be expressed in terms of a and a^\dagger and is given by

$$H = \hbar\omega(X_0^2 + P_0^2) = \hbar\omega(a^\dagger a + \frac{1}{2}\mathbb{1}). \quad (8)$$

Note that the eigenvalue problem for the Hamiltonian can now be expressed as an eigenvalue problem for the so called number operator

$$N = a^\dagger a, \quad (9)$$

which is of the form

$$N|\psi\rangle = \left(\frac{E}{\hbar\omega} - \frac{1}{2}\right)|\psi\rangle. \quad (10)$$

Furthermore, all eigenvalues (if there are any) of N are non-negative, because if $|\psi\rangle$ is an eigenvector of N with eigenvalue n , then

$$n = n\langle\psi|\psi\rangle = \langle\psi|N\psi\rangle = \langle a\psi|a\psi\rangle \geq 0.$$

The commutation relations of the ladder operators with the number operator can easily be evaluated:

$$[N, a] = -a \quad \text{and} \quad [N, a^\dagger] = a^\dagger. \quad (11)$$

So, if $|\psi_n\rangle$ is a normalized eigenstate of N with eigenvalue n , then, assuming $a|\psi_n\rangle$ and $a^\dagger|\psi_n\rangle$ don't vanish, $a|\psi_n\rangle$ is again an eigenstate of N with eigenvalue $n - 1$ (and $a^\dagger|\psi_n\rangle$ is an eigenstate of N with eigenvalue $n + 1$). In other words,

$$a|\psi_n\rangle = \sqrt{n}|\psi_{n-1}\rangle \quad (12)$$

and

$$a^\dagger|\psi_n\rangle = \sqrt{n+1}|\psi_{n+1}\rangle. \quad (13)$$

The proportionality constants follow from the requirement that the $|\psi_n\rangle$ are normalized and from the relations

$$\langle a\psi_n|a\psi_n\rangle = \langle\psi_n|N|\psi_n\rangle = n\langle\psi_n|\psi_n\rangle$$

and

$$\langle a^\dagger \psi_n | a^\dagger \psi_n \rangle = \langle \psi_n | (N + [a, a^\dagger]) | \psi_n \rangle = (n + 1) \langle \psi_n | \psi_n \rangle.$$

Consider now the equation $a|\psi\rangle = 0$ in the x -representation, i.e.

$$\left(\sqrt{\frac{m\omega}{2\hbar}} x + \sqrt{\frac{\hbar}{2m\omega}} \frac{\partial}{\partial x} \right) \psi(x) = 0. \quad (14)$$

This equation has a unique normalizable solution $\psi_0(x) \propto e^{-\frac{m\omega x^2}{2\hbar}}$. On the other hand, the equation $a^\dagger|\psi\rangle = 0$ doesn't have a normalizable solution. We have therefore obtained a set of normalized solutions $\{|\psi_n\rangle | n \geq 0\}$ (these states are called the number states) of the eigenvalue problem 10, given by

$$|\psi_n\rangle = \frac{1}{\sqrt{n!}} (a^\dagger)^n |\psi_0\rangle. \quad (15)$$

These are in fact already all the solutions of this eigenvalue problem, because if there were a different set of solutions $\{|\phi_n\rangle\}$, then $a|\phi_n\rangle < 0$ for some n . We therefore have a unique state of lowest energy, $|\psi_0\rangle$, with a non-zero energy

$$E_0 = \frac{\hbar\omega}{2}. \quad (16)$$

The expectation values of position and momentum vanish, as is expected from the correspondence principle, but the variances are finite. The same statement holds for all the other number states. To get more familiar "classical" states (i.e. states, whose position/momentum expectation values are non-zero and follow the classical trajectories), we have to consider superpositions of number states. The coherent state is defined by $a|\psi_\alpha\rangle = \alpha|\psi_\alpha\rangle$ and can be expressed as a superposition of number states:

$$|\psi_\alpha\rangle = e^{-\frac{1}{2}|\alpha|^2} \sum_{n=0}^{\infty} \frac{\alpha^n}{\sqrt{n!}} |\psi_n\rangle.$$

Note that α is in general complex (it corresponds to the complex amplitudes, which we have already used several times) and we can write

$$\alpha = |\alpha|e^{i\phi}.$$

With this notation, the expectation values for position and momentum are obtained as

$$\langle \psi_\alpha | X_0 | \psi_\alpha \rangle = |\alpha| \cos \phi$$

and

$$\langle \psi_\alpha | P_0 | \psi_\alpha \rangle = |\alpha| \sin \phi.$$

For $\phi = \phi_0 + \omega t$ the expectation values thus follow the classical trajectories. However, there is now an inherent uncertainty characterized by the variances

$$(\Delta X_0)^2 = (\Delta P_0)^2 = \frac{1}{4}.$$

Note that in SI units (i.e. for X and P instead of X_0 and P_0) we obtain

$$\Delta X \cdot \Delta P = \frac{\hbar}{2}$$

and the Heisenberg uncertainty relation is fulfilled.

1.2 Classical description of optomechanical systems

1.2.1 The electromagnetic field

In classical physics light is described as an electromagnetic wave, i.e. by two time-dependent coupled fields (the electric field \vec{E} and the magnetic field \vec{H}). The fields (and their coupling) arise mathematically as solutions to the Maxwell equations¹. In free space, the Maxwell equations are given by

$$\nabla \cdot \vec{E} = 0, \quad (17)$$

$$\nabla \cdot \vec{H} = 0, \quad (18)$$

$$\nabla \times \vec{E} = -\mu_0 \frac{\partial}{\partial t} \vec{H}, \quad (19)$$

$$\nabla \times \vec{H} = \epsilon_0 \frac{\partial}{\partial t} \vec{E}. \quad (20)$$

In these equations ϵ_0 and μ_0 are constants known as the electric permittivity and the magnetic permeability of free space. Note that the Maxwell equations already imply the wave equations for all the components of both \vec{E} and \vec{H} :

$$\Delta u = \frac{1}{c^2} \frac{\partial^2}{\partial t^2} u \quad (21)$$

where u stands for an arbitrary component of either the electric or the magnetic field. Also note that, since Maxwell's equations are linear, the superposition of an arbitrary number of solutions is again a solution. As we will see, this has the important consequence that all (physical) solutions can be obtained as a superposition of particularly simple solutions oscillating at a fixed frequency.

The energy density of an electromagnetic field in free space is given by

$$\rho = \frac{1}{2}(\epsilon_0 \vec{E}^2 + \mu_0 \vec{H}^2) \quad (22)$$

and the corresponding conservation law is

$$\frac{\partial \rho}{\partial t} = -\nabla \cdot \vec{S}$$

with

$$\vec{S} = \vec{E} \times \vec{H}.$$

The energy flux density \vec{S} is also known as the Poynting vector. Another important quantity is the intensity $I = |\langle \vec{S} \rangle_t|$, where $\langle \cdot \rangle_t$ denotes a time-average (taken over a time long compared to an optical period). The (linear) momentum density of the electromagnetic wave is given by

$$\vec{P} = \frac{1}{c^2} \vec{S}. \quad (23)$$

¹James Clerk Maxwell obtained these equations in 1865 as modifications to the equations used to describe the static fields (and Faraday's law), after noticing inconsistencies in the old equations. Many of the consequences of his theory were not experimentally verified until years later.

For more details see any book about electrodynamics, e.g. [6]. Consider now an electromagnetic wave of the form

$$\vec{E}(\vec{x}, t) = \text{Re} \left[\vec{E}_0(\vec{x}) e^{-i\omega t} \right], \quad \vec{H}(\vec{x}, t) = \text{Re} \left[\vec{H}_0(\vec{x}) e^{-i\omega t} \right]. \quad (24)$$

Such a wave oscillates at a fixed frequency ω and is therefore called monochromatic. Note that we will mostly use the complex quantities for calculations. The corresponding real quantities are obtained by taking the real part of the expression in question after the evaluation. Since this wave has to satisfy the Maxwell equations, it follows that the components of \vec{E}_0 and \vec{H}_0 obey the so called Helmholtz equation

$$\Delta u + k^2 u = 0, \quad (25)$$

where $k = \frac{\omega}{c}$ and u denotes any component of \vec{E}_0 or \vec{H}_0 . Note that any physical solution can be obtained as sum/integral over monochromatic waves by means of Fourier analysis (this is shown in section 1.3.1).

We will often encounter monochromatic waves of the form (note that the Helmholtz equation is fulfilled for $|\vec{k}| = \frac{\omega}{c}$)

$$\vec{E}(\vec{x}, t) = \text{Re} \left[\vec{E}_0 e^{-i(\omega t - \vec{k} \cdot \vec{x})} \right], \quad \vec{H}(\vec{x}, t) = \text{Re} \left[\vec{H}_0 e^{-i(\omega t - \vec{k} \cdot \vec{x})} \right]. \quad (26)$$

Waves of this form are called plane waves, the vector \vec{k} is called wave vector (its magnitude is called wave number) and determines the direction of propagation. Again, more general waves can be analyzed by considering them as superpositions of plane waves with different wave vectors \vec{k} and different frequencies ω (see section 1.3.1).

Substituting the expression for the plane wave in the Maxwell equations 19 and 20, we obtain

$$\vec{k} \times \vec{E} = -i\mu_0\omega\vec{H}, \quad \vec{k} \times \vec{H} = i\epsilon_0\omega\vec{E} \quad (27)$$

It follows that the fields and the wave vector \vec{k} are mutually perpendicular. We also obtain the relations

$$|\vec{k}| = \omega\sqrt{\mu_0\epsilon_0} = \frac{2\pi}{\lambda}, \quad (28)$$

where λ denotes the wavelength, and

$$\frac{|E|}{|H|} = \sqrt{\frac{\mu_0}{\epsilon_0}} \approx 377\Omega. \quad (29)$$

The Poynting vector for a plane wave is parallel to the wave vector \vec{k} and the intensity is given by

$$I = \langle \vec{S} \rangle_t = \frac{1}{2} |E_0| |H_0| = \frac{|E_0|^2}{\eta} \quad (30)$$

with

$$\eta = 2\sqrt{\frac{\mu_0}{\epsilon_0}}.$$

Due to the simple relation between the electric and the magnetic field of a plane wave, it is usually sufficient to consider only one of the fields (by convention the electric field) during calculations and we will from now on do so.

1.2.2 Optical cavities

An optical cavity is, generally expressed, a device which confines (stores) electromagnetic radiation. In practice this is usually realized by two or more mirrors (see figure 4). From now on we only consider Fabry-Perot cavities, i.e. cavities made from two parallel mirrors. Due to interference and the boundary conditions at the mirrors, a stationary field in an ideal cavity takes the form of standing waves and the wavelength is restricted to certain discrete numbers. As an example consider two perfect mirrors separated by a distance l

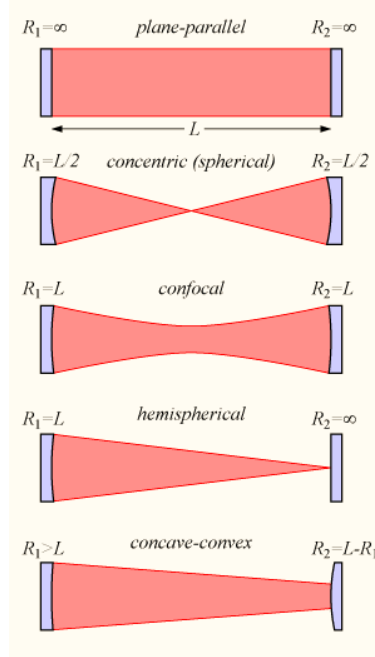


Figure 4: Different configurations of optical cavities. Figure originally published on the English wikipedia by Bob Mellish under the terms of the GNU Free Documentation License.

along the x -axis and assume a monochromatic field $\vec{E}(\vec{x}, t) = \text{Re} \left[\vec{E}_0(\vec{x}) e^{-i\omega t} \right]$ is present in the cavity. We furthermore assume the direction of propagation is perpendicular to the mirrors and that the electric field has purely transverse components. The solutions to the Helmholtz equation (with the boundary condition $\vec{E}_0(x=0) = \vec{E}_0(x=l) = 0$) are of the form

$$\vec{E}_0(\vec{x}) = \vec{E}_0(y, z) \sin(kz)$$

with

$$k = n \frac{\pi}{l}, \quad n \in \mathbb{Z}.$$

The general solution is a linear superposition of such terms. In terms of the angular frequency $\omega = kc$, this quantization condition reads

$$\omega = n \frac{\pi c}{l}$$

and these frequencies are called the resonance frequencies of the cavity. The separation between adjacent resonance frequencies,

$$\Delta\omega = \frac{\pi c}{l}, \tag{31}$$

is called the free spectral range of the cavity.

If we include losses in our model, this strict condition on the frequency (wave number, wavelength) will be relaxed. The permitted frequencies (wave numbers, wavelengths) will no longer be quantized, but rather have a certain distribution (as we will see, peaked at and symmetric around the resonance frequencies). I am going to assume that the different polarization modes don't couple (this is a good assumption for many types of cavities, for a more general analysis see e.g. [11]) and for convenience I am going to omit the vector sign on the electric fields from now on.

Denote the amplitude reflectivity/transmission coefficients of the mirrors by $r_1, r_2/t_1, t_2$ (the intensity reflection/transmission coefficients are therefore given by r_i^2/t_i^2 and $r_i^2 + t_i^2 = 1$). The first mirror (r_1, t_1) is the input mirror, i.e. an external field, which is assumed to be a plane wave with amplitude E_{in} (it is sufficient to only consider the electric field, as discussed in the last section) and angular frequency ω_L , is incident upon it. We are interested in the reflected field (amplitude E_r), the field in the cavity and the output field (i.e. the field transmitted through the second mirror, amplitude E_{out}). I choose a phase convention such that the reflection of the input field on the first mirror results in a phase shift of π , while an internal reflection doesn't (see e.g. [9]). Denote the amplitude of the electric field (traveling in positive x-direction) in the cavity directly after the input mirror by E_{cav} . Now consider first the act of cavity filling: Assume that for $t < 0$ all fields are zero and for $t \geq 0$ $E_{in} = \text{const} \neq 0$. Then, for $0 \leq t < \frac{2L}{c}$, the intracavity amplitude directly after the first mirror is given by $E_{cav}^0 = t_1 E_{in}$. For $\frac{2L}{c} \leq t < \frac{4L}{c}$ we get $E_{cav}^1 = E_{cav}^0(1 + r_1 r_2 e^{i\delta\phi})$, i.e. the intracavity field is now given as a superposition between the transmitted input field and the field still in the cavity after one round trip. The phase picked up by the field during one round trip is given by $\delta\phi = \frac{2L}{c}\omega_L$. The steady-state value of the intracavity field amplitude can therefore be expressed as a convergent infinite series,

$$E_{cav} = \sum_{i=0}^{\infty} E_{cav}^0 \gamma^i = \frac{1}{1 - \gamma} E_{cav}^0,$$

where $\gamma = r_1 r_2 e^{i\delta\phi}$. The intracavity intensity is given by

$$I_{cav} = \frac{|E_{cav}|^2}{2\eta} = \frac{I_{in} t_1^2}{1 + r_1^2 r_2^2 - 2\text{Re}[\gamma]} = \frac{I_{in} t_1^2}{(1 - r_1 r_2)^2} \frac{1}{1 + \left(\frac{2F}{\pi}\right)^2 \sin^2\left(\frac{\delta\phi}{2}\right)}, \quad (32)$$

where

$$F = \frac{\pi \sqrt{r_1 r_2}}{1 - r_1 r_2}$$

is called the finesse of the cavity. It is easy to see that the intracavity intensity has maximum values at the resonance frequencies of the corresponding ideal cavity (given by equation 31). While an ideal cavity can only confine light at these precise frequencies, a realistic cavity will have a non-zero intracavity field at all frequencies. However, any radiation which is not close to a resonance frequency experiences strong attenuation. Optical cavities are therefore often used as frequency filters (they can of course also be used as spatial filters, if their geometry can only sustain certain spatial modes) or spectrum analyzers.

The intensity and phase distributions of the reflected field and the output field can be obtained from the relations

$$E_r = -r_1 E_{in} + r_2 t_1 e^{i\delta\phi} E_{cav} = \frac{\gamma - r_1^2}{r_1(1 - \gamma)} E_{in}$$

and

$$E_{out} = t_2 e^{-i\frac{\delta\phi}{2}} E_{cav} = \frac{t_1 t_2 e^{-i\frac{\delta\phi}{2}}}{1 - \gamma} E_{in}.$$

Of particular interest for us is the phase difference between the input field and the reflected field, which is given by

$$\phi_r = \arg\left(\frac{\gamma - r_1^2}{r_1(1 - \gamma)}\right).$$

The intensity/phase distributions of the intracavity field and the reflected field are plotted in figure 5.

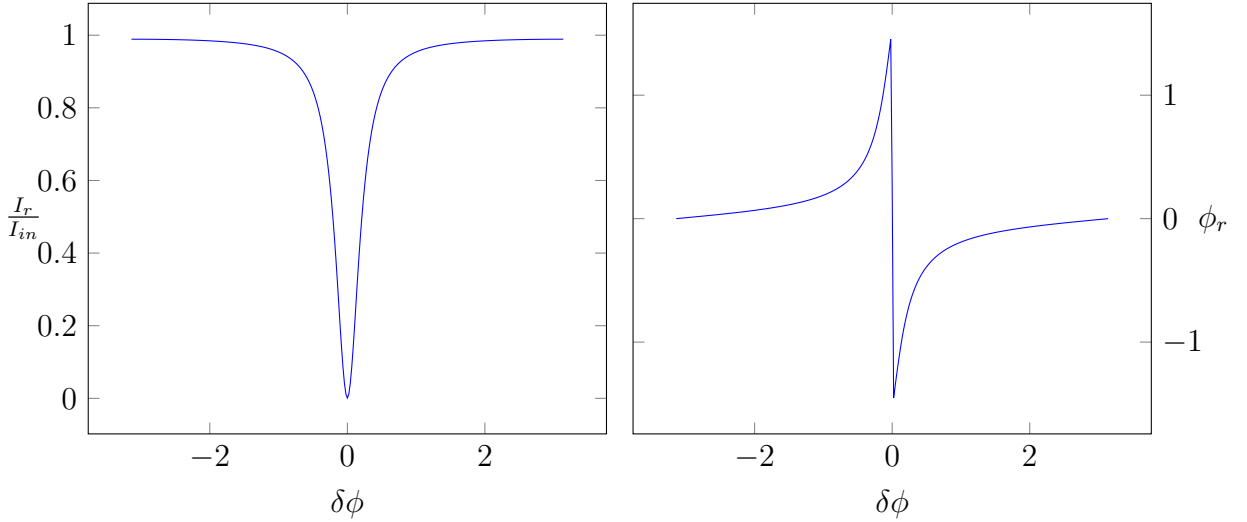


Figure 5: Intensity and phase distributions of the reflected field for a cavity with $r_1 = r_2 = 0.9$.

We are now properly prepared to derive the general "equations of motions" for the fields (often referred to as input-output formalism) and to treat cavity filling and cavity decay. Given an input field with amplitude $E_{in}(t)$ (matched to the geometry of the cavity), the cavity field (E_{cav} now denotes the amplitude directly before the input mirror traveling in negative x-direction, since this makes the calculations clearer) fulfills the relation

$$E_{cav}(t + \tau) = \gamma E_{cav}(t) + t_1 r_2 e^{i\delta\phi} E_{in}(t), \quad (33)$$

where $\tau = \frac{2l}{c}$ denotes the cavity round-trip time. Since τ is usually small compared to other timescales (e.g. modulation of the input field/mirror position, time resolution of a measurement), we can replace this equation with the corresponding differential equation, i.e. making the approximation

$$\dot{E}_{cav}(t) = \frac{E_{cav}(t + \tau) - E_{cav}(t)}{\tau}.$$

To further simplify this expression and to obtain consensus with the notation used in the field of quantum optomechanics, we assume from now on that the frequency input field is close to a resonance frequency of the cavity (i.e. $e^{i\delta\phi} \approx 1 + i\delta\phi$) and that $t_i^2 \ll 1$, such that $r_i \approx 1 - \frac{t_i^2}{2}$. Inserting this approximations in equation 33 and neglecting all terms which contain a prefactor of the form $t_i^2 \delta\phi$ or $t_i t_j^2$, we arrive at

$$\dot{E}_{cav}(t) = \left(i\frac{\delta\phi}{\tau} - \frac{t_1^2 + t_2^2}{2\tau}\right) E_{cav}(t) + \frac{t_1}{\tau} E_{in}(t).$$

Usually one defines the cavity decay rate $\kappa := \kappa_1 + \kappa_2$ with $\kappa_i = \frac{t_i^2}{\tau}$ (in the next paragraph it should become clear why this is called cavity decay rate) and uses that $\delta\phi = \tau\omega = \tau(\omega - \omega_c) = \tau\Delta \pmod{2\pi}$, since $\tau\omega_c = n2\pi$, where Δ is called the detuning. The equation of motion for the cavity field then simply reads

$$\dot{E}_{cav}(t) = (i\Delta - \frac{\kappa}{2})E_{cav}(t) + \sqrt{\frac{\kappa_1}{\tau}}E_{in}(t).$$

The amplitude of the incident field is often normalized by $E_{in} \rightarrow \frac{1}{\sqrt{\tau}}E_{in}$ (we will see the reason for this in the next subsection), in which case one gets

$$\dot{E}_{cav}(t) = (i\Delta - \frac{\kappa}{2})E_{cav}(t) + \sqrt{\kappa_1}E_{in}(t). \quad (34)$$

This is the form one most often finds in the literature (usually for the corresponding quantum equation). Note that losses other than mirror losses (e.g. scattering of light out of the cavity) can be included by simply adding another term to the cavity decay rate (formally such losses aren't any different than the losses at the second mirror).

An immediate application is cavity decay, i.e. we assume the input field is "switched off" at some time t_0 . Then we can solve the differential equation

$$\dot{I}_{cav}(t) = -\kappa I_{cav}(t)$$

with $I_{cav}(0) = I_0$ and get the solution

$$I_{cav}(t) \approx I_0 e^{-\kappa t}.$$

Note that (with the approximations we made, i.e. high reflectivity mirrors, small detuning) there are a lot of different equally valid forms for the equations. We have chosen here the "conventional" form, i.e. the form which is most often used in the literature.

Also, formulating the equations of motion for the (slowly-changing) amplitudes instead for the fields is called working in the rotating frame (or sometimes - wrongly - called the rotating wave approximation) and corresponds (classically) to a transformation $e^{i\omega t}$.

With these approximations and the corresponding notation, we can reformulate the relations for the intracavity intensity and the reflected field. First note that

$$E_{cav}(\omega) = \frac{\sqrt{\kappa_1}}{\frac{\kappa}{2} - i(\Delta + \omega)}E_{in}(\omega)$$

and therefore the average intensity is

$$I_{cav} = \frac{\kappa_1}{\frac{\kappa^2}{4} + \Delta^2}I_{in}.$$

The reflected field (normalized by $E_r \rightarrow \frac{1}{\sqrt{\tau}}E_r$) can now be written as

$$E_r = \sqrt{\kappa_1}E_{cav} - E_{in}.$$

1.2.3 Optomechanics

We will treat classical optomechanics by means of the prototypical optomechanical system (figure 6): Consider an optical cavity in which one of the mirrors is perfect and a mechanical oscillator, while the other mirror is partially transparent. A plane wave with

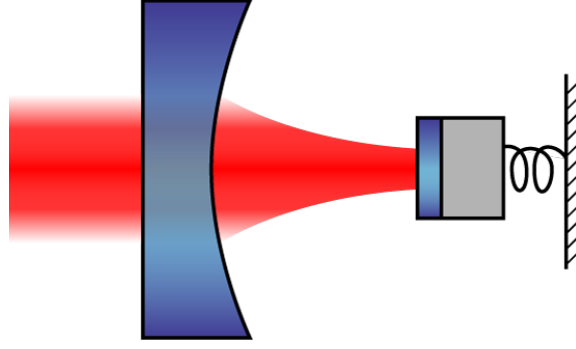


Figure 6: Typical optomechanical system. Figure originally published on the english wikipedia by the user Schmoele under the terms of the "Creative Commons Attribution-Share Alike 3.0 Unported" license.

constant amplitude and angular frequency ω_L is incident on the partially transparent mirror. A field in such a cavity will be in dynamic interplay with the mirror position: On the one hand, the phase of the radiation reflected at the mirror and therefore also the intracavity intensity (since the intensity depends on the phase, as we have seen in the last section) depends on the position of the mirror; on the other hand, the field will effect radiation pressure on the mirror and thus the position of the mirror depends on the intensity in the cavity.

We will now express these dynamics in mathematical form and discuss some important properties of such a system.

From eq. 23 and eq. 30 it follows that the momentum transferred to the mirror per round trip is just $4\frac{V}{c^2}I$, where V denotes the volume of the cavity and I is the intensity (in SI units). The momentum transferred per unit time, i.e. the force on the mirror, is then given by $\frac{4V}{\tau c^2}I = \frac{2V}{lc}I$, where l denotes the length of the cavity (note that the dependence of the force on the cavity length l is strictly through the intensity, as $\frac{V}{l}$ is independent of l).

Redefining the intracavity field as $E_{cav} \rightarrow \sqrt{\frac{V\epsilon_0}{\hbar\omega_L}} E_{cav}$, we can write the force on the mirror as

$$F_{rad} = \frac{\hbar\omega_L}{l} |E_{cav}|^2.$$

Note that $|E_{cav}|^2 = \frac{\int_V dV \rho}{\hbar\omega_L}$ (with ρ is given by equation 22) corresponds in the quantum mechanical picture to the (mean) number of photons in the cavity².

The reaction of the intracavity intensity to a change in mirror position isn't instantaneous but determined by the cavity decay rate. To determine the full dynamics of the optomechanical system we assume that the mirror oscillates around some equilibrium position and that the oscillations $x(t)$ are small compared to the mean length of the cavity L . We also take τ from now to denote the mean cavity round trip time and we redefine the amplitude of the incident field by $E_{in} \rightarrow \sqrt{\frac{V\epsilon_0}{\tau\hbar\omega_L}} E_{in}$, which means that $\hbar\omega_L |E_{in}|^2$ is the incident power in SI-units (i.e. in the quantum mechanical picture $|E_{in}|^2$ is the rate of incident photons). The equation of motion for the cavity fields then takes the form of equation 34. We now expand $\omega_{cav}(x) = n\frac{\pi c}{L+x}$ to the first power of x (i.e. $\omega_{cav}(x) = \omega_{cav}(1 - \frac{x}{L})$) with

²Note that in most treatments of cavity optomechanics the radiation pressure force is written as $\frac{\hbar\omega_{cav}}{l} |E_{cav}|^2$ and also $|E_{cav}|^2 = \frac{\int_V dV \rho}{\hbar\omega_{cav}}$. This is allowed as in these treatments a high finesse cavity is assumed.

$\omega_{cav} = n \frac{\pi c}{L}$) and arrive at the equation

$$\dot{E}_{cav} = \left(i \left(\Delta + \frac{\omega_{cav}}{L} x \right) - \frac{\kappa}{2} \right) E_{cav} + \sqrt{\kappa_1} E_{in}. \quad (35)$$

Together with the corresponding equation of motion for the mechanical oscillator, which, according to the preceding discussion, can be written as

$$m_{eff}(\ddot{x} + \gamma \dot{x} + \omega_M^2 x) = \frac{\hbar \omega_L}{L} |E_{cav}|^2, \quad (36)$$

we now have two coupled equations which describe the dynamics of the system. For a discussion of the effective mechanical mass m_{eff} see section 3.6.

The second equation is often written with the intensity defined as $I = \frac{|E_{cav}|^2}{\tau}$ (i.e. the rate of photons incident on the mirror) and then reads

$$m_{eff}(\ddot{x} + \gamma \dot{x} + \omega_M^2 x) = 2\hbar k I.$$

In the frequency domain this becomes

$$x(\omega) = 2\hbar k \chi(\omega) I(\omega).$$

One effect of the radiation pressure force is a static average shift in the cavity length, given by

$$x_{st} = 2\hbar k \chi(0) \langle I(t) \rangle,$$

where $\langle . \rangle$ is again a time average.

The non-linear equations 35 and 36 are in general not analytically solvable. However, it often makes sense to assume that the field amplitudes E_{in} and E_{cav} fluctuate around some mean value \bar{E}_{in} resp. \bar{E}_{cav} and that the magnitude of the fluctuations is small compared to the mean values. Furthermore, to achieve consensus with the usual notation, we will from now on assume a high-finesse cavity and write $F_{rad} = \frac{\hbar \omega_{cav}}{L} |E_{cav}|^2$. Inserting $E_{in} = \bar{E}_{in} + \delta E_{in}$, $E_{cav} = \bar{E}_{cav} + \delta E_{cav}$ in the non-linear equations and neglecting all terms of the form $\delta E_i \delta E_j$ and $x \delta E_i$, we get the steady state solution for the mean intracavity field,

$$\bar{E}_{cav} = \frac{\sqrt{\kappa_1}}{\frac{\kappa}{2} - i\Delta} \bar{E}_{in},$$

as well as the linearized equations

$$\delta \dot{E}_{cav} = \left(i\Delta - \frac{\kappa}{2} \right) \delta E_{cav} + i \frac{\omega_{cav}}{L} x \bar{E}_{cav} + \sqrt{\kappa_1} \delta E_{in} \quad (37)$$

and

$$m_{eff}(\ddot{x} + \gamma \dot{x} + \omega_M^2 x) = \frac{2\hbar \omega_{cav}}{L} \text{Re}[\bar{E}_{cav}^* \delta E_{cav}]. \quad (38)$$

Note that in equation 38 we have already made the substitution $x \rightarrow x_{st} + x$, where x_{st} denotes the (static) shift in the equilibrium position of the cavity due to the mean intensity:

$$x_{st} = \frac{\hbar \omega_{cav}}{m_{eff} \omega_M^2 L} |\bar{E}_{cav}|^2.$$

The linear equations are the starting point for most optomechanics discussions, both in the classical and in the quantum regime (for a short introduction to non-linear dynamics, see e.g. [13]). In particular, one can explain cooling (and heating) of the mechanical motion in this picture by solving the equations (including the thermal force) in the frequency domain and obtaining a modified mechanical susceptibility, which in a certain parameter regime leads to attenuation (cooling) or amplification (heating) of the thermal motion. It is important to note that this is a purely classical effect, in contrast to cooling with the pulsed scheme (see section 4).

1.3 Quantum mechanical description of optomechanical systems

In this section I'm going to introduce the quantum mechanical treatment of optomechanics. The first subsection superficially covers the quantum mechanical theory of electromagnetic radiation (for a more in-depth treatment see e.g. [8]), after that we are going to apply that formalism to the interaction of light with a (single mechanical mode of a) moving mirror in a cavity.

1.3.1 Quantum electrodynamics

In order to pass from classical mechanics to quantum mechanics in the canonical way we have to use the Hamiltonian formalism for the classical theory, i.e. we have to find a Hamiltonian such that the field equations arise as the usual Hamilton equations. This is possible for the electromagnetic theory, but only for fields enclosed in a finite volume. However, since the volume can be chosen arbitrarily large, the resulting theory does not depend on the size of this volume.

We will begin with the well-known statement that the electric and magnetic fields in vacuum can be represented by a single quantity known as the vector potential (in the Coulomb gauge) and usually denoted by \vec{A} . The derivation of the following results is outside of the scope of this thesis and therefore I refer readers unfamiliar with these results to any textbook about classical electrodynamics, e.g. [6] or [12]. The electric and magnetic fields are related to \vec{A} by

$$\vec{E} = -\frac{\partial}{\partial t}\vec{A}$$

and

$$\vec{H} = \frac{1}{\mu_0}\nabla \times \vec{A}.$$

Any component of the vector potential satisfies the wave equation. Therefore (compare to the quantization of the electric field in section 1.2.2), if we consider the field in a cube with volume $V = L^3$ and choose periodic boundary conditions for \vec{A} and its derivatives, we can express the vector potential as the infinite sum

$$\vec{A}(\vec{x}, t) = \sum_{\vec{k}, \lambda} \vec{e}_{\vec{k}, \lambda} (A_{\vec{k}, \lambda}(t) e^{i\vec{k}\vec{x}} + A_{\vec{k}, \lambda}^*(t) e^{-i\vec{k}\vec{x}}),$$

where $\vec{k} = \frac{2\pi}{L}\vec{n}$ and the components of \vec{n} are integers. $\vec{e}_{\vec{k}, \lambda}$ denotes the polarization of the mode and $\lambda \in \{0, 1\}$. The polarization vectors for a given mode are normalized and perpendicular both to each other and to the wave vector \vec{k} of the mode (the last fact follows from the Coulomb condition for the vector potential). The wave equation for the components of the vector potential translates to

$$\frac{\partial^2}{\partial t^2} A_{\vec{k}, \lambda}(t) = -c^2 k^2 A_{\vec{k}, \lambda}(t) = -\omega_k^2 A_{\vec{k}, \lambda}(t),$$

which is formally equivalent to the equation of motion for a harmonic oscillator. From now on we take as the solution to this equation $A_{\vec{k}, \lambda}(t) = A_{\vec{k}, \lambda} e^{-i\omega t}$. Then, the energy of the fields in the cubic volume,

$$E = \frac{1}{2} \int_V dV (\epsilon_0 \vec{E}^2 + \mu_0 \vec{H}^2),$$

can be expressed in terms of $x_{\vec{k},\lambda} := A_{\vec{k},\lambda}(t) + A_{\vec{k},\lambda}^*(t)$ and $p_{\vec{k},\lambda} := \frac{d}{dt}x_{\vec{k},\lambda}$ as

$$E = \frac{1}{2}\epsilon_0 V \sum_{\vec{k},\lambda} (p_{\vec{k},\lambda}^2 + \omega_k^2 x_{\vec{k},\lambda}^2).$$

We can thus treat every mode of the electromagnetic field (confined to periodic boundary conditions in a box) as a harmonic oscillator. The quantization of (every mode of) the field now proceeds in exact analogy to the quantization of the harmonic oscillator performed in section 1.1.2. For a complete derivation and a more detailed discussion of the Hamiltonian form of the electromagnetic theory see e.g. [8] or [12]. To establish a connection between this derivation and the expressions given in section 1.2, calculate the electric field as

$$\vec{E}(\vec{x}, t) = -\frac{\partial}{\partial t} \vec{A}(\vec{x}, t) = \sum_{\vec{k},\lambda} \vec{e}_{\vec{k},\lambda} (i\omega A_{\vec{k},\lambda} e^{-i(\omega t - \vec{k}\vec{x})} - i\omega A_{\vec{k},\lambda}^* e^{i(\omega t - \vec{k}\vec{x})}).$$

This also shows that the electric field can indeed be written as a superposition of plane waves and, even though this is strictly speaking only valid for fields enclosed in some volume with appropriate boundary conditions, one is free to choose the volume and the boundary conditions as necessary for the physical situation.

The rest of this section treats the quantum theory of radiation, capital letters will denote operators. After the quantization one can write down the Hamiltonian in terms of the usual creation/annihilation operators, i.e.

$$H = \sum_{\vec{k},\lambda} \hbar\omega_k (a_{\vec{k},\lambda}^\dagger a_{\vec{k},\lambda} + \frac{1}{2}),$$

which are related to the operators corresponding to the vector potential coefficients by

$$a_{\vec{k},\lambda} = \sqrt{\frac{\hbar}{2\epsilon_0 V \omega_k}} A_{\vec{k},\lambda}$$

and

$$a_{\vec{k},\lambda}^\dagger = \sqrt{\frac{\hbar}{2\epsilon_0 V \omega_k}} A_{\vec{k},\lambda}^*.$$

For experiments taking place in a physical cavity one can choose the 'quantization volume' to coincide with the volume of the cavity, in one dimension and taking one mode this of course reproduces the results of section 1.2.2).

1.3.2 Quantum optomechanics

We have already seen in the last section, that the Hamiltonian of an electromagnetic field confined to an ideal cavity (and a good model for a high finesse cavity with an single excited mode and fixed polarization) is given by

$$H = \hbar\omega_{cav} a^\dagger a,$$

where ω_{cav} denotes a resonance frequency of the cavity and a, a^\dagger the familiar annihilation/creation operators. If one of the end mirrors of the cavity acts as a harmonic oscillator, we have to add a similar term for it and also account for the dependence of the optical frequency on the position of the mirror. Classically, $\omega_{cav}(x)$ (x denoting the displacement

of the moving mirror from its equilibrium position) is given by equation 31. Furthermore, if the oscillations of the mirror are small compared to the mean cavity length L , we can approximate $\omega_{cav}(x) \approx \omega_{cav}(0) + \frac{d\omega_{cav}(x)}{dx}x \approx \omega_{cav}(0) - \frac{\omega_{cav}}{L}x$. We will from now on denote $\omega_{cav}(0)$ as ω_{cav} and carrying over to the quantum regime, we arrive at the Hamiltonian

$$H = \hbar\omega_{cav}a^\dagger a + \hbar\omega_M b^\dagger b - \hbar\frac{\omega_{cav}}{L}x_0 X_M a^\dagger a$$

with ω_M being the mechanical frequency and b, b^\dagger denoting the annihilation/creation operators of the mechanical system. Note that x_0 is determined by the choice of units for the operator $X_M = b + b^\dagger$. Using the same convention as in section 1.1.2 (note however the difference by a factor of $\frac{1}{2}$ in the definition of the quadratures X_M resp. X_0), we have $x_0 = \sqrt{\frac{\hbar}{2m\omega_M}}$. The expression $\frac{\omega_{cav}}{L}x_0$ is often denoted by g_0 and called the single photon optomechanical coupling strength. We have also assumed that the free spectral range of the cavity is much larger than the mechanical frequency and neglected any coupling to other cavity modes. The Hamiltonian of our optomechanical system thus consists of two harmonic oscillator terms and the interaction term

$$H_{int} = -\hbar g_0(b + b^\dagger)a^\dagger a.$$

A full derivation of the Hamiltonian by the canonical procedure is given in [10].

The corresponding Heisenberg equations of motion for the operators a and b are given by

$$\dot{a} = -i(\omega_{cav} - g_0 X_M)a$$

and

$$\dot{b} = -i\omega_M b + ig_0 a^\dagger a.$$

The equation for the optical "field" simply describes harmonic evolution with the phase modulation caused by the oscillating mirror. Taking the expectation values and switching to the rotating frame, one recovers the classical equation 35 (for a perfect cavity, i.e. $\kappa = \kappa_1 = 0$). The equation for the mechanical annihilation operator is easier to interpret if we write down the corresponding equations for the position and momentum operators (in SI-units), namely

$$\dot{X}_M^{SI} = \frac{1}{m}P_M^{SI}$$

and

$$\dot{P}_M^{SI} = -m\omega_M^2 X_M^{SI} + \hbar\frac{\omega_{cav}}{L}a^\dagger a.$$

These are just the classical equations of motion for a harmonic oscillator already including the momentum transfer due to the electromagnetic field.

So far we have assumed a perfect cavity, i.e. no optical losses and no mechanical dissipation. These loss mechanisms are formulated on the basis of quantum Langevin equations, i.e. they are modeled as an interaction with an infinite bath of harmonic oscillators. The resulting equations for a and b are given by

$$\dot{a} = -i\omega_{cav}a + ig_0 X_M a - \frac{\kappa}{2}a + \sqrt{\kappa}a_{in} \quad (39)$$

and

$$\dot{b} = -i\omega_M b + ig_0 a^\dagger a - \frac{\gamma}{2}b. \quad (40)$$

The first equation can be easily understood: As before, the first two terms simply describe the harmonic evolution of the field and the phase modulation due to the change in cavity length. The third term gives the decay and the fourth term describes the coupling to the incident field. Taking the expectation values and switching to the rotating frame, one obtains the classical equation for the electric field amplitude (equation 35, assuming no intracavity losses and perfect reflectivity of the back mirror, i.e. $\kappa = \kappa_1$ in the notation of section 1.2).

The first and second terms of the equation for the mechanical annihilation operator account for the harmonic evolution and the momentum transfer to the mechanical oscillator, the third term accounts for mechanical dissipation. Note that this treatment of dissipation is valid only for $\frac{\gamma}{2\omega} \ll 1$ and in that case one recovers the classical equations (for the position/momentum operators in SI units) by taking the expectation values (compare with section 1.1.1).

It is often convenient to work in a frame rotating at the laser frequency ω_L , which corresponds to the treatment given in section 1.2. The Hamiltonian in the new frame reads

$$H = -\hbar\Delta a^\dagger a + \hbar\omega_M b^\dagger b - \hbar g_0 X_M a^\dagger a,$$

where we have again used the detuning $\Delta = \omega_L - \omega_{cav}$. An important case is $\omega_L = \omega_{cav}$ (i.e. “driving the cavity on resonance”), which is primarily used for interferometric position measurements and which we will use later on in the pulsed scheme. The Hamiltonian (in the rotating frame) in this case is simply given by

$$H = \hbar\omega_M b^\dagger b - \hbar g_0 X_M a^\dagger a. \quad (41)$$

Now we write

$$a = \bar{a} + \delta a$$

with \bar{a} denoting the expectation value of a^3 , i.e. for a given optical state $|\psi\rangle$, $\bar{a} = \langle\psi|a|\psi\rangle$. For high \bar{a} (e.g. for strong coherent states) we can drop all terms in the interaction Hamiltonian which are of second order in δa . This is often called the linear approximation. With this notation and the linear approximation the interaction Hamiltonian reads

$$H_{int} = -\hbar g_0 X_M (\bar{a}^\dagger \bar{a}) - \hbar g_0 X_M (\bar{a}^\dagger \delta a + \delta a^\dagger \bar{a}).$$

The first term simply corresponds to an average radiation pressure force (and resulting mean shift of the mirror position) and therefore vanishes, if we shift the coordinate system appropriately. Furthermore, w.l.o.g., we can choose \bar{a} to be real. The Hamiltonian then reads

$$H = \hbar\omega_{cav} a^\dagger a + \hbar\omega_M b^\dagger b - \hbar g_0 \sqrt{\bar{n}} X_M (\delta a^\dagger + \delta a), \quad (42)$$

where $\bar{n} = \bar{a}^\dagger \bar{a} = \bar{a}^2$ is the mean number of photons in the cavity.

The equations of motions for the cavity field introduced here will be the starting point of our treatment of pulsed cavity optomechanics in appendix A and we will use a procedure similar to the linearization here to simplify the theory.

³Strictly speaking, one should write $a = \bar{a}\mathbb{1} + \delta a$ with $\mathbb{1}$ denoting the identity operator. However, the identity operator is customarily omitted in the literature.

2 Quantum measurements and quantum state tomography

The standard treatment of quantum mechanics describes a pure quantum state by a wave function (and a mixed state by a density operator), which is related to the probability of obtaining certain measurement outcomes. For example, if some (point) particle can be described by a wave function $\psi(\vec{x}, t)$ (in the position representation), then the probability of finding that particle in the volume V' at the time T is given by $\int_{V'} |\psi(\vec{x}, T)|^2 dV$. By preparing many particles in the same quantum state and repeatedly measuring the position one can reconstruct the probability distribution $|\psi(\vec{x}, T)|^2$ with (in principle) arbitrary accuracy.

However, knowing just the probability distribution for a single observable (e.g. position) doesn't allow us to reconstruct the quantum state (i.e. the wave function/density operator). Consider as an example a wave function

$$\psi(x) \propto e^{x^2 + i2p'x},$$

i.e. a coherent state. Measuring the probability distribution (of position measurement outcomes) gives us access to the absolute value, but doesn't tell us anything about the complex argument of the wave function. Taking the Fourier transform, which in natural units is given by $\psi(p) = \frac{1}{\sqrt{\pi}} \int dx \psi(x) e^{-i2px}$, we obtain the wave function in the momentum representation

$$\psi(p) \propto e^{-(p-p')^2}.$$

This tells us, that by measuring the distributions of both position and momentum, we can obtain the absolute value and the complex argument of the wave function and therefore completely reconstruct the state. The reconstruction of quantum states by measuring probability distributions of certain observables is called quantum state tomography and treated in more detail in the next section.

In the discussion above we have left two questions unanswered. The first one is: "What happens to the particle (or, more specifically, its quantum state) during a measurement?" or rather "What is the quantum state directly after a measurement?". While this question can be readily answered for observables with a discrete spectrum and ideal measurements (e.g. spin states, which can be measured with perfect accuracy in a magnetic field), the answer is not as straightforward for e.g. position measurements, which always have a measurement dependent resolution. There are, I believe, two reasons for neglecting this question in the usual textbook treatment of quantum mechanics. The first one is simplicity and the second one is historic: In the olden days measurements on ensembles of quantum states and the reconstruction of such states was the main focus of scientists (most likely because measurement techniques in these times were not advanced enough to repeatedly measure properties of a single quantum object).

The other question we haven't answered yet is "How can one prepare an ensemble of quantum states?", i.e. how is it possible to repeatedly prepare a given quantum state (and how can one know that the object is indeed in this state)? We will focus on one possibility to do quantum state preparation, which is strongly related to the first question. As we will see, by measuring an observable of a quantum state it is possible to know (from the result of the measurement) what the quantum state after the measurement is.

The action of measurements on a quantum state and the possibility of using such measurements to prepare quantum states are the subject of the section after the next one.

2.1 Quantum tomography

In this section we consider how one can experimentally determine a quantum state. For this we first recall in this section that a general quantum state is characterized by its density operator and then introduce in the next section an equivalent description via the so called Wigner function, which is more closely related to actual experimental measurements of continuous variables (i.e. the probability distributions).

We then outline how the Wigner function can be obtained from a finite set of measurements via the (numerical implementation of the) inverse radon transform.

So far in our treatment we have mostly considered pure quantum states, which are represented by wave functions. In classical mechanics, the analogue to this would be a point in phase space, which fully describes a physical system. However, as we know, it is not always feasible or even possible to consider the exact state of an arbitrary system (e.g. for some finite volume filled with a gas consisting of millions of particles one would have to know the position and momentum of each particle as well as the exact nature of the interactions between the particles and the boundary conditions describing the behaviour of the particles at the boundary of the volume). In classical mechanics a workaround for this problem is given by statistical mechanics, the art of finding the probabilities that a physical system behaves in a certain way. The same methods can be applied to quantum mechanics, i.e. we can describe an arbitrary state of a quantum system by stating the probabilities that this system is in one of multiple possible pure quantum states.

Mathematically this is done by introducing the density operator ρ of the system as

$$\rho = \sum_n p_n |\psi_n\rangle\langle\psi_n|.$$

Here, ψ_n is a possible pure state of the system and p_n gives the probability that the system is in this state. In particular,

$$\sum_n p_n = 1.$$

Note that, while the ψ_n 's are assumed to be normalized, they don't have to be orthogonal. The sum can be either finite or infinite, depending on the state. If the possible states aren't described by a discrete parameter but by a continuous one, we can write

$$\rho = \int ds p(s) |\psi(s)\rangle\langle\psi(s)|,$$

where $p(s)$ is a probability function on the interval of integration (usually \mathbb{R}).

It is straightforward to see that the probability of obtaining a measurement outcome q , when measuring an observable Q (with discrete or continuous spectrum), is given by $\langle q|\rho|q\rangle$. The expectation value can be expressed as $\text{Tr}(\rho Q)$.

If the Hamiltonian can be diagonalized, i.e. if we can find a basis $\{\psi_n|n \in \mathbb{N}\}$, such that $H|\psi_n\rangle = E_n|\psi_n\rangle$, then we can define the matrix elements of the density operator as

$$\rho_{nm} = \langle\psi_n|\rho|\psi_m\rangle.$$

An important example for the use of a density operator is the thermal state (i.e. the state of a system in thermal equilibrium with its environment). According to classical statistical mechanics, we can write the probability for such a system to have the energy E as $e^{-\frac{1}{k_B T} E}$, where k_B is the Boltzmann constant and T is the temperature⁴. If the Hamiltonian H of

⁴Note that this isn't valid for all systems in thermal equilibrium - e.g. for systems of identical fermions one has to use Fermi-Dirac statistics, since some energy states are forbidden by the Pauli exclusion principle.

the system has non-degenerate eigenvalues E_n , the density matrix is given as

$$\rho^{th} = \frac{\sum_n e^{-\frac{1}{k_B T} E_n} |\psi_n\rangle \langle \psi_n|}{\sum_n e^{-\frac{1}{k_B T} E_n}} = \frac{e^{-\frac{1}{k_B T} H}}{Tr(e^{-\frac{1}{k_B T} H})}. \quad (43)$$

The matrix elements are therefore given by

$$\rho_{nm}^{th} = \frac{e^{-\frac{E_n}{k_B T}}}{Tr(e^{-\frac{1}{k_B T} H})} \delta_{nm},$$

i.e. the density matrix for a thermal state is diagonal and (assuming $E_n > E_m$ for $n > m$) the diagonal elements are Boltzmann distributed.

Consider as an example the quantum harmonic oscillator. The expectation value of the number operator is given by

$$\bar{n} := Tr(a^\dagger a \rho) = \frac{\sum_n n e^{-\frac{\hbar \omega n}{k_B T}}}{\sum_n e^{-\frac{\hbar \omega n}{k_B T} E_n}} = (e^{\frac{\hbar \omega}{k_B T}} - 1)^{-1}. \quad (44)$$

The expectation values of both the position and momentum quadrature vanish, their variances are given by

$$(\Delta X)^2 = (\Delta P)^2 = \frac{1}{2}(\bar{n} + \frac{1}{2}). \quad (45)$$

One can now use the equipartition theorem (equation 4) to find the relation between the temperature T and the mean thermal occupation \bar{n} , in SI-units

$$T = \frac{\hbar \omega_M}{k_B} (\bar{n} + \frac{1}{2}). \quad (46)$$

For large \bar{n} this of course agrees with the value for T obtained by the explicit inversion of equation 44.

The above results will be used in section 4 (with a slightly different definition of the mechanical quadratures, s.t. $(\Delta X_M)^2 = (\Delta P_M)^2 = 2\bar{n} + 1$) to determine the resulting state after a pulsed measurement on an initial thermal state.

2.1.1 The Wigner function

The Wigner function has arisen from the desire to do quantum mechanical calculations in phase space (in analogy to classical statistical mechanics). While it cannot be interpreted as a probability distribution on phase space (since it may take negative values), it still has many properties of probability functions and also has been proven extremely useful for providing graphical illustrations of quantum states and plotting experimental results. I advise anyone who wishes to understand the Wigner function on a deeper level to read Wigner's original paper [14].

The Wigner function for a wave function and for one degree of freedom is defined as

$$W(x, p) = \frac{1}{h\pi} \int_{-\infty}^{\infty} ds e^{i\frac{2ps}{\hbar}} \psi^*(x+s) \psi(x-s)$$

or, using the Dirac notation,

$$W(x, p) = \frac{1}{h\pi} \int_{-\infty}^{\infty} ds e^{i\frac{2ps}{\hbar}} \langle x+s | \psi \rangle \langle \psi | x-s \rangle.$$

It follows directly that integration with respect to p (resp. x) gives the probability densities for x (resp p):

$$P(x) := |\psi(x)|^2 = \int_{-\infty}^{\infty} dp W(x, p),$$

$$P(p) := |\psi(p)|^2 = \int_{-\infty}^{\infty} dx W(x, p).$$

This also implies normalization, i.e.

$$\int_{-\infty}^{\infty} dx \int_{-\infty}^{\infty} dp W(x, p) = 1$$

and, furthermore, we can express the expectation value of any function of the form $f(x, p) = g(x) + h(p)$ (where g, h are piecewise integrable functions on \mathbb{R}) with the help of the Wigner function as

$$\int_{-\infty}^{\infty} dx \int_{-\infty}^{\infty} dp f(x, p) W(x, p).$$

For a quantum state described by a density operator

$$\rho = \sum_n p_n |\psi_n\rangle \langle \psi_n|,$$

we can define the Wigner function as the sum over the pure state Wigner functions, i.e.

$$W(x, p) = \sum_n W_n(x, p),$$

where $W_n(x, p)$ denotes the Wigner function for the pure state ψ_n . With this definition the relevant properties of the Wigner function (normalization, giving probability distributions after integration over x, p , etc..) remain unchanged. Note that the Wigner function for a general state can be written as

$$W(x, p) = \frac{1}{h\pi} \int_{-\infty}^{\infty} ds e^{i\frac{2ps}{h}} \langle x + s | \rho | x - s \rangle.$$

Figure 7 shows the Wigner functions of various states of a harmonic oscillator as a function of x and p (in natural units).

2.1.2 Reconstruction of the Wigner function

As we have seen in the last section, the Wigner function contains all the information of a quantum state, i.e. knowledge of the Wigner function fully characterizes a quantum state. The aim of this section is to outline how one can reconstruct the Wigner function of a quantum state. A necessary requirement is that one can prepare the same state repeatedly to measure the statistical properties (i.e. the probability distributions). To start, we define the rotated quadrature observables (compare to section 2)

$$X_\phi = X \cos(\phi) + P \sin(\phi).$$

If X and P are the quadrature operators of a light mode, then X_ϕ can be directly measured by homodyne detection, as outlined in the next section. In that case ϕ is the phase

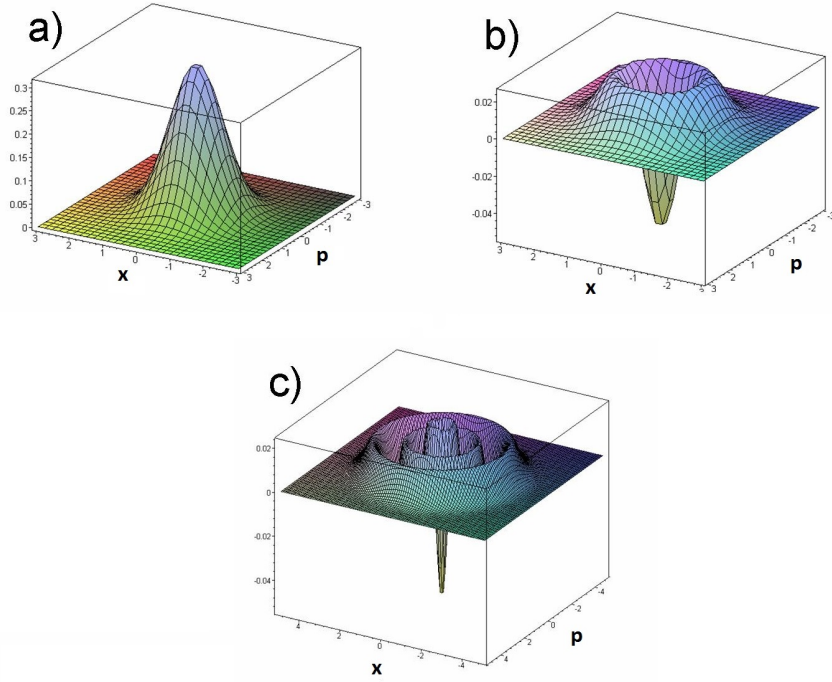


Figure 7: Wigner functions of (a)the vacuum state, (b)the $n = 1$ number state and (c)the $n = 5$ number state.

difference between the local oscillator and the signal beam.

One can show [15], that the probability distribution $P(x_\phi)$ can be obtained by integrating the Wigner distribution over the conjugate variable p_ϕ , i.e.

$$P(x_\phi) = \int_{-\infty}^{\infty} dp_\phi W\left(x_\phi \cos(\phi) - p_\phi \sin(\phi), x_\phi \sin(\phi) + p_\phi \cos(\phi)\right)$$

and that there is a one-to-one correspondence between the set probability distributions $\{P(x_\phi) \mid \phi \in [0, \pi)\}$ and the Wigner function. The explicit inversion (inverse Radon transformation) is however of limited use for practical applications. If, as in a typical experimental situation, the probability distribution is measured only for a finite number of values of ϕ , one can still reconstruct the Wigner function by using a numerical implementation of the inverse Radon transformation. One possibility to do this is to group the obtained measurement results (for each rotated quadrature) in bins and then to apply the filtered back-projection algorithm as described in [24]. Most numerical computing packages already contain an implementation of this algorithm. In our measurement scheme described in section 4.2.2 we used the MATLAB-function "iradon" to perform the inversion.

2.2 Quantum measurement

Before we start with the theory of quantum measurements, I am going to write a few words about the difference between fundamental uncertainties in quantum mechanics and perturbations due to measurements. The Heisenberg uncertainty relation states that the values of two canonically conjugate observables cannot be known at the same time with perfect accuracy. This is a statement about fundamental uncertainties - no matter, how the state was prepared, one cannot know the values corresponding to both observables with better accuracy. The Heisenberg uncertainty relation stems from the wave

description of quantum mechanics and the fact that the bandwidth $\Delta\omega$ of a wave packet and its duration τ are related by⁵ $\Delta\omega\tau \geq 1$. Take as an example again a point particle and consider its position-momentum uncertainty relation (in SI-units) $\Delta x\Delta p \geq \frac{\hbar}{2}$. One simple consequence of this relation is the fact that we need to measure the distributions of the position and the momentum (of an ensemble of identically prepared particles) to reconstruct the particle state, as we have already seen above. The other direct consequence already hints at state preparation. Assume that the particle is in a state with $\Delta x\Delta p = \frac{\hbar}{2}$ and assume that we can measure the position with an accuracy δx better than Δx . Then the quantum state after the measurement will have an increased momentum spread $\delta p \geq \frac{\hbar}{2\delta x}$, such that the new quantum state fulfills $\delta x\delta p \geq \frac{\hbar}{2}$. The minimum momentum spread $\frac{\hbar}{2\delta x}$ occurs independent of the exact nature of the position measurement (although most measurements lead to a perturbation of the momentum orders of magnitude higher than the minimum perturbation).

This fact is often expressed as another uncertainty relation, which states that a measurement of an observable X with measurement accuracy Δx_{meas} is inevitably accompanied by a perturbation Δp_{pert} in the canonically conjugate variable P , such that $\Delta x_{meas}\Delta p_{pert} \geq \frac{\hbar}{2}$.

2.2.1 Quantum measurement theory

The standard textbook treatment of quantum measurement consists of the wave function collapse formalism introduced first by von Neumann. This formalism is only strictly applicable to observables with a discrete spectrum (e.g. spin), which can be measured with perfect measurement accuracy. Assume we have an observable Q with eigenvectors $\{|\psi_n\rangle \mid n \in \mathbb{N}\}$ and corresponding eigenvalues $\{q_n \mid n \in \mathbb{N}\}$. For simplicity we also assume that Q is non-degenerate (i.e. all eigenvalues are distinct). As the eigenstates of Q form a (orthonormal) basis of the Hilbert space, any state $|\psi\rangle$ of our quantum system can be written as a linear superposition of the eigenstates, i.e.

$$|\psi\rangle = \sum_n c_n |\psi_n\rangle,$$

where $c_n = \langle\psi_n|\psi\rangle$ and $|\psi\rangle$ is assumed to be normalized, which corresponds to $\sum_n |c_n|^2 = 1$. The von Neumann formalism postulates that an ideal measurement of Q will result in a measurement outcome q_n with probability $|\langle\psi_n|\psi\rangle|^2 = |c_n|^2$ and that the state of our system after the measurement will be $|\psi_n\rangle$.

Note that an actual experimental measurement (even of an observable with discrete spectrum) cannot necessarily be described by this formalism. For example, the photon number observable of a cavity mode has a discrete spectrum and can be measured by absorbing the photons, which leaves the cavity mode in the vacuum state.

The von Neumann formalism can easily be expanded to systems with two or more degrees of freedom. The Hilbert space of the complete system is given by the tensor product of the Hilbert spaces belonging to each degree of freedom. For now on we will only consider systems with two degrees of freedom (corresponding to Hilbert spaces V_1 and V_2) and we will use the notation

$$|\psi, \varphi\rangle = |\psi\rangle \otimes |\varphi\rangle$$

⁵Here $\frac{\Delta\omega}{2\pi}$ is the standard deviation in frequency and $\frac{1}{2}v\tau$, v being the group velocity of the wave, is the standard deviation in position. The wave uncertainty relation given here is only strictly valid for special cases (which includes most “familiar” waveforms), a general treatment is more complicated. See e.g. [7].

for a product state in the tensor space $V = V_1 \otimes V_2$ (where $|\psi\rangle \in V_1$ and $|\varphi\rangle \in V_2$). States of this form are also called separable. Note that a basis of the tensor space is given by $\{|\psi_i, \varphi_j\rangle \mid i, j \in \mathbb{N}\}$, where the $|\psi_i\rangle$ and $|\varphi_i\rangle$ form a basis V_1 and V_2 , respectively. An important feature of the tensor space is that there are states $|\Phi\rangle = \sum_{i,j} |\psi_i, \varphi_j\rangle$, which cannot be expressed as product states. Such a state is said to be entangled.

The scalar products defined in V_1 and V_2 can be extended to a scalar product in V by

$$\langle \psi, \varphi | \psi', \varphi' \rangle = \langle \psi | \psi' \rangle \langle \varphi | \varphi' \rangle.$$

So far the von Neumann formalism applies directly (we have a Hilbert space with a scalar product corresponding to measurement probabilities). However, we now also have to consider what happens to a state of the system if a measurement is performed on just one degree of freedom, while the other is left unperturbed. Let Q and O be two observables on V_1 and V_2 with non-degenerate discrete spectrum and eigenstates $|\psi_n\rangle$ and $|\varphi_n\rangle$, respectively. Any state $|\Phi\rangle$ in the tensor space can then be expressed as $|\Phi\rangle = \sum_{n,m} c_{nm} |\psi_n, \varphi_m\rangle$. If a measurement is performed on only one of the subsystems, e.g. Q is measured, then the measurement result will be an eigenvalue q_n of Q with probability $\sum_m |\langle \psi_n, \varphi_m | \Phi \rangle|^2 = \sum_m |c_{nm}|^2$ and the state of the system will be

$$\frac{1}{N} \sum_m \langle \psi_n, \varphi_m | \Phi \rangle |\psi_n, \varphi_m\rangle = \frac{1}{N} \sum_m c_{nm} |\psi_n, \varphi_m\rangle = |\psi_n\rangle \otimes \frac{1}{N} \sum_m c_{nm} |\varphi_m\rangle,$$

where $N = \sqrt{\sum_m |c_{nm}|^2}$ ensures normalization. The resulting state after the measurement will therefore be a product state and the subsystem the measurement was performed on will be in an eigenstate of the corresponding observable. The state of the other subsystem is

$$\frac{1}{N} \sum_m \langle \psi_n, \varphi_m | \Phi \rangle |\varphi_m\rangle = \frac{1}{N} \sum_m c_{nm} |\varphi_m\rangle.$$

In particular, if the initial state was a product state, the state of the other subsystem will be unaffected.

We will now start with the treatment of measurements on continuous observables, in which the uncertainty of the measurement outcomes is in general due to both the fundamental uncertainty intrinsic to quantum states and a measurement error introduced by the measurement apparatus (depending on the exact nature of the measurement). In this and the subsequent chapter we will closely follow the description of measurements given in [7] in chapters 2 and 3.

Assume that we want to measure an observable Q of some quantum system described by a wave function $|\psi_{in}\rangle$. We will characterize the measurement apparatus by the conditional probability distribution $w(\tilde{q}|q)$ describing the probability of obtaining a measurement outcome \tilde{q} , if the quantum system is in an eigenstate $|q\rangle$. Note that such eigenstates generally don't exist in the Hilbert space, but they are formally defined (in the Dirac notation) by the relations $\langle q | \psi \rangle = \psi(q)$ and $\langle q' | q \rangle = \delta(q - q')$ (i.e. as functionals and distributions).

The probability of obtaining a measurement outcome \tilde{q} is given by

$$\begin{aligned} w(\tilde{q}) &= \int_{-\infty}^{\infty} dq w(\tilde{q}|q) |\psi_{in}(q)|^2 \\ &= \text{Tr}(W(\tilde{q}) |\psi_{in}\rangle \langle \psi_{in}|) \end{aligned}$$

with

$$W(\tilde{q}) := \int_{-\infty}^{\infty} dq w(\tilde{q}|q) |q\rangle \langle q|.$$

If the quantum system is initially in a mixed state described by a density operator (see section 2.1) ρ_{in} , we have

$$\begin{aligned} w(\tilde{q}) &= \int_{-\infty}^{\infty} dq w(\tilde{q}|q) \langle q|\rho_{in}|q\rangle \\ &= \text{Tr}(W(\tilde{q}) \rho_{in}). \end{aligned}$$

To be able to make some statements about the state of the system after obtaining a measurement outcome \tilde{q} we assume for now (we will derive this in the next section for a certain type of measurement) that the state after the measurement can be written in the form

$$|\psi_{out}\rangle = \frac{1}{\sqrt{w(\tilde{q})}} \Omega(\tilde{q}) |\psi_{in}\rangle. \quad (47)$$

Normalization of the state then requires that

$$\Omega(\tilde{q})^\dagger \Omega(\tilde{q}) = W(\tilde{q})$$

and we can therefore write

$$\Omega(\tilde{q}) = U(\tilde{q}) W^{\frac{1}{2}}(\tilde{q}),$$

where we have defined

$$W^{\frac{1}{2}}(\tilde{q}) := \int_{-\infty}^{\infty} dq \sqrt{w(\tilde{q}|q)} |q\rangle\langle q|$$

and $U(\tilde{q})$ is a unitary operator (i.e. $U^\dagger(\tilde{q})U(\tilde{q}) = \mathbb{1}$). Mathematically at least, a measurement (that can be described by equation 47) can thus be represented as a two step procedure

$$|\psi_{in}\rangle \rightarrow |\psi'\rangle = \frac{1}{\sqrt{w(\tilde{q})}} W^{\frac{1}{2}}(\tilde{q}) |\psi_{in}\rangle \rightarrow |\psi_{out}\rangle = U(\tilde{q}) |\psi'\rangle.$$

As $[W^{\frac{1}{2}}(\tilde{q}), Q] = 0$, the first step doesn't perturb the measured quantity. The unitary operator $U(\tilde{q})$ depends on the exact nature of the measurement. If $[U(\tilde{q}), Q] = 0$ as well (i.e. Q is left unperturbed by the measurement), one speaks of a quantum non-demolition (QND) measurement.

The same treatment can be applied to mixed states, leading to

$$\rho_{in} \rightarrow \rho' = \frac{1}{w(\tilde{q})} W^{\frac{1}{2}}(\tilde{q}) \rho_{in} W^{\frac{1}{2}}(\tilde{q}) \rightarrow \rho_{out} = U(\tilde{q}) \rho' U^\dagger(\tilde{q}).$$

It is instructive to note that

$$\langle q|\rho'|q\rangle = \frac{1}{w(\tilde{q})} w(\tilde{q}|q) \langle q|\rho_{in}|q\rangle.$$

As the second step of the measurement is a unitary process, this is already probability distribution of the state after the measurement. In particular, if the distribution corresponding to the initial state did not contain any features smaller than the width of the distribution $w(\tilde{q}|q)$, the distribution corresponding to the final state is entirely determined by the measurement procedure, i.e. by $w(\tilde{q}|q)$.

2.2.2 Indirect measurements

Most measurements on quantum systems can be classified as either a direct or indirect measurement. A direct measurement is one in which the quantum system interacts directly with a classical measurement apparatus (e.g. a photographic plate). In a direct measurement the quantum object is generally perturbed by a much higher amount than required by the uncertainty relation, often the quantum state is even irreversibly lost (e.g. absorption of a photon).

In an indirect measurement one utilizes a second quantum system, called the quantum probe, to perform a measurement on the first quantum system. The quantum probe is prepared in some desired initial state and then interacts with the system (the interaction is governed by the usual laws of quantum mechanics, i.e. the Schrodinger equation), before an observable of the quantum probe is measured in a direct measurement. As the interaction will generally result in entanglement between the two systems, this will also provide us with information on the first quantum system.

Furthermore, as the measurement on the quantum probe is direct and can therefore be performed with high measurement accuracy (which we will assume from now on), the only source of error is due to the fundamental uncertainties of the quantum probe. We will now derive equation 47 for an indirect measurement by assuming that the measurement on the probe's observable is exact (which is a valid assumption as long as the measurement error is small compared to the initial uncertainties in the probe's state). This assumption allows us to use the von Neumann formalism for the measurement on the quantum probe (replacing the sums with integrals as we now consider observables with continuous spectra).

For simplicity we assume for now that both the quantum system and the quantum probe are in a pure state at the begin of the interaction. We denote the initial states of the probe and the system by

$$|\psi_{in}\rangle = \int dp \psi_{in}(p) |p\rangle$$

and

$$|\varphi_{in}\rangle = \int dq \varphi_{in}(q) |q\rangle,$$

respectively. As the initial states are separable, we can write the state of the combined system as

$$|\Phi_{in}\rangle = |\psi_{in}, \varphi_{in}\rangle = \int dp \int dq \psi_{in}(p) \varphi_{in}(q) |p, q\rangle.$$

After the interaction, the state of the combined system will be given by

$$|\Phi_{out}\rangle = U|\Phi_{in}\rangle,$$

where U is a unitary operator describing the interaction between the probe and the system. Note that U is completely determined by its action on the 'basis states' $|p, q\rangle$, i.e. by the coefficients β appearing in $U|p, q\rangle = \int dp' \int dq' \beta(p, q, p', q') |p', q'\rangle$.

Note that, since the measurement on the quantum probe is regarded to be exact, the probability distribution of obtaining a measurement outcome \tilde{p} is

$$w(\tilde{p}) = \int d\tilde{q} |\langle \tilde{p}, \tilde{q} | \Phi_{out} \rangle|^2.$$

After the measurement on the quantum probe has produced a measurement outcome \tilde{p} , the final state of the quantum system is

$$|\varphi_{out}\rangle = \frac{1}{N} \int d\tilde{q} \langle \tilde{p}, \tilde{q} | \Phi_{out} \rangle |\tilde{q}\rangle = \frac{1}{N} \int dq \varphi_{in}(q) \int dq' \beta(q, q'; \tilde{p}) |q'\rangle$$

with

$$\beta(q, q'; \tilde{p}) := \int dp \psi_{in}(p) \beta(p, q, \tilde{p}, q')$$

and $N = \sqrt{w(\tilde{p})}$. We can therefore define an operator $\Omega(\tilde{p})$ by

$$\Omega(\tilde{p}) |q\rangle = \int dq' \beta(q, q'; \tilde{p}) |q'\rangle,$$

such that

$$|\varphi_{out}\rangle = \frac{1}{\sqrt{w(\tilde{p})}} \Omega(\tilde{p}) |\varphi_{in}\rangle$$

and this equation takes the form of equation 47. If the quantum system is initially in a mixed state described by a density operator ρ_{in} , then the state after the measurement is

$$\rho_{out} = \frac{1}{w(\tilde{p})} \Omega(\tilde{p}) \rho_{in} \Omega^\dagger(\tilde{p}).$$

3 Experimental techniques

In this section we will introduce some of the more technical aspects necessary to understand our experiment. One aim here is to connect the theory introduced so far to the actual implementation in an experiment and to show that the application of this theory is valid for our experimental setup. Another aim is to introduce the most important components used in the setup and explain their working principle.

3.1 Lasers and electromagnetic beams

Up until now in our treatment we have mostly considered both electromagnetic radiation and harmonic oscillators to be one-dimensional. For obvious reasons actual radiation and actual resonators aren't one-dimensional. This section is reserved for a motivation of this treatment for electromagnetic radiation (and provide references for further reading), a justification of this treatment for the harmonic oscillator and the interaction of radiation with such an oscillator will be given in section 3.6.

Even though many aspects of laser theory are closely related to concepts presented in this thesis (for example, the monochromatic properties of laser light stem from the fact that a cavity can only support discrete wavelengths and the frequency noise of a laser stems directly from noise in the length of the laser cavity), a deep treatment of lasers is outside the scope of this thesis. I therefore refer the interested reader to the comprehensive treatment given in [16] and below I will only motivate the results most important for the purpose of this thesis.

To justify our theoretical treatment, a laser used in experiments described by our treatment has to fulfill three conditions. First, the laser should be monochromatic and second, the frequency shouldn't change over some given duration (determined by the exact nature of the experiment). Highly stabilized laser systems have a long term absolute frequency stability better than 1 part in 10^{10} with a bandwidth of the order of a few hertz [16], so these conditions are fulfilled. These properties imply excellent temporal coherence of electromagnetic radiation produced by such a laser.

The third property the laser should have is transverse spatial coherence. This allows us to write the (complex) electric field produced by a laser as

$$\vec{E}(x, y, z, t) = v(y, z) \vec{E} e^{-i(\omega t - kx)},$$

where x denotes the coordinate along the propagation direction and y, z denote coordinates in the plane transverse to the propagation direction. If all optical component in the experiment are linear and isotropic, and furthermore if the transverse spatial distribution $v(y, z)$ is small compared to the dimensions of the optical components (and in particular any photodetectors), then $v(y, z)$ can be integrated over and absorbed in the amplitude, so we get the familiar expression

$$\vec{E}(x, t) = \vec{E} e^{-i(\omega t - kx)}$$

for the complex electric field at the output port of the laser. For a more detailed treatment of the interaction of electromagnetic radiation with a moving mirror see section 3.6.

Most single mode lasers fulfill these criteria, to cite from [16]:

A single-transverse-mode laser oscillator can produce (usually in practice, and always in principle) an output beam that is more or less uniform in amplitude and constant in phase ("uniphase") across its full output aperture of width or diameter d .

Any Gaussian beam will spread during propagation, but this doesn't affect the statements

above. Also, the Rayleigh range (distance after which the cross sectional area of the beam is twice the original area) of a single mode laser is sometimes much larger than the propagation distance through the experiment. One can also choose to use fiber optics (as we have done in our experiment), which of course prohibits any spread of the beam during propagation. So called single mode fibers don't affect the transverse distribution and temporal coherence properties of the beam, also they have very little loss. For more information on fiber optics see e.g. [17].

A quantum mechanical treatment of such beams of light is done best by choosing an appropriate quantization volume. In most experiments the path between laser and detector cannot be considered an actual cavity and therefore we characterize the light by a continuous distribution of wavevectors parallel to the direction of beam propagation. This corresponds to choosing a quantization volume of infinite length in propagation direction but finite cross section perpendicular to the propagation direction. Performing the quantization and assuming that only a narrow bandwidth of frequencies (wavevectors) is excited around a central frequency ω (as we just have seen this is true for many laser systems), one finds annihilation/destruction operators such that

$$a^\dagger(t)a(t) = \frac{P(t)}{\hbar\omega},$$

where $P(t)$ denotes the operator corresponding to the optical power. The operator $a^\dagger a$ is now called the photon flux operator. For a more detailed treatment see [8]. From now on it is understood that the annihilation/destruction operators are defined in this way. We will from now on also always use the corresponding normalization for the classical fields, i.e. $P(t) = \hbar\omega|E(t)|^2$ (with $P(t)$ being the optical power).

Note that this treatment is valid also for electromagnetic pulses as long as the narrow bandwidth approximation is fulfilled (i.e. the pulses can't be too short).

3.2 Interferometry

Optical interferometry refers to a method which uses the correlations of (partially) coherent light beams between two space-time points to measure the phase difference between these two points. It can, in turn, also be used to measure the degree of coherence between two space-time points. A more specific method, which is used quite often, is to separate an incident beam, then expose one of the sub-beams to a phase shift relative to the other sub-beam (e.g. a different path length) and then recombine the two sub-beams. The electric fields of the two sub beams are superposed and, if the light is correlated, this results in either amplification (constructive interference) or attenuation (destructive interference) of the electric field.

3.3 The beam splitter

The beam splitter is one of the key components in most optical interferometric experiments. The working principle of a beam splitter is that two incident beams are brought to spatially overlap (and therefore interfere), after which the beam is split in two separate beams again. Beam splitters can be manufactured in many different ways, a particularly easy one is to simply glue two glass prisms together. To determine the behaviour of a specific beam splitter one would in principle have to consider the behaviour of electromagnetic waves when traveling through the respective materials. However, assuming that the materials are linear and that the beam splitter is approximately loss-less (in modern beam splitters a relative loss of 10^{-4} to 10^{-2} is common), one can simply treat the beam

splitter as a black box with two incoming beams E_1, E_2 and two outgoing beams E_3, E_4 (see figure 8), which are related by a linear transformation, i.e.

$$\begin{pmatrix} E_3 \\ E_4 \end{pmatrix} = BS \begin{pmatrix} E_1 \\ E_2 \end{pmatrix} = \begin{pmatrix} c_{13} & c_{23} \\ c_{14} & c_{24} \end{pmatrix} \begin{pmatrix} E_1 \\ E_2 \end{pmatrix},$$

where the matrix components are in general complex. We will from now on assume that the E_i 's are the amplitudes of a plane wave at the entry port/output port of the beam splitter. We can then determine the behaviour of general electromagnetic waves by considering them as a superposition of plane waves.

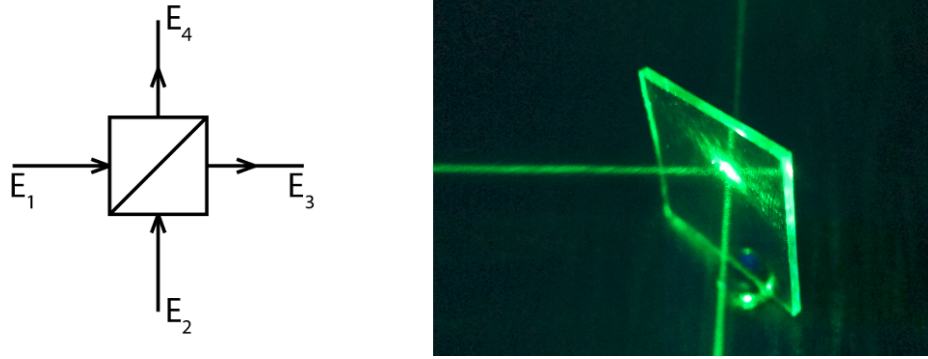


Figure 8: Symbolic image of a beam splitter (left) and picture of an aluminum coated glass plate used as a beam splitter (right).

The condition that the beam splitter is loss-less translates to

$$|E_1|^2 + |E_2|^2 = |E_3|^2 + |E_4|^2$$

and therefore

$$|c_{13}|^2 + |c_{14}|^2 = |c_{23}|^2 + |c_{24}|^2 = 1$$

and

$$c_{13}c_{23}^* = c_{14}c_{24}^* = 0.$$

Writing $c_{nm} = |c_{nm}|e^{i\phi_{nm}}$ and using the expressions above, we arrive at

$$\phi_{13} + \phi_{24} - \phi_{23} - \phi_{14} = \pi$$

and

$$|c_{13}| = |c_{24}|, \quad |c_{23}| = |c_{14}|.$$

Using $t := |c_{13}|$ and $r := |c_{14}|$, the transformation matrix can be written as

$$BS = \begin{pmatrix} t & -r \\ r & t \end{pmatrix}.$$

For obvious reasons t is denoted transmittance and r is denoted reflectivity.

If we need to describe the electromagnetic fields by quantum theory, most of the above is still valid, we only have to replace the plane wave electric field amplitudes E_i with the single mode annihilation operators a_i . The main difference to the classical beam splitter model shows when only one of the input ports is illuminated. In the classical theory one would simply set the corresponding amplitude to zero, while in the quantum theory the input is in the vacuum state and has to be considered in the calculations.

The beam splitter model is not only useful for describing physical beam splitters in an experiment, but also for describing losses of other optical components. This will be used in the next section to provide a realistic model for photodetectors.

3.4 Photodetectors

A photodetector is an intensity detector, i.e. it measures not the electric (or magnetic) field directly, but only the intensity of the light (field measurements using photodetectors can nevertheless be done using interferometry, see the next section). For low intensities a photodetector therefore acts as a photon counter and the practical implementation for photodetectors is quite different depending on the field strength. For example, in semiconductor photodiodes the photoeffect is used to create electron-hole pairs which, under the application of an electric field, constitute a current which can then be measured. In the single photon regime this current would be far too weak to reliably measure, so one has to use other methods. A particularly simple method - used in the avalanche photodiode - is to just increase the applied voltage - once the kinetic energy of the single electron freed due to the absorption of a photon is high enough it will free other charge carriers in collisions, creating an "avalanche" of electrons which can be measured. Of course such a system saturates easily (i.e. enters a non-linear regime) and can't be used for high intensities.

Here we will focus on the properties of photodetectors made for measuring high (rela-

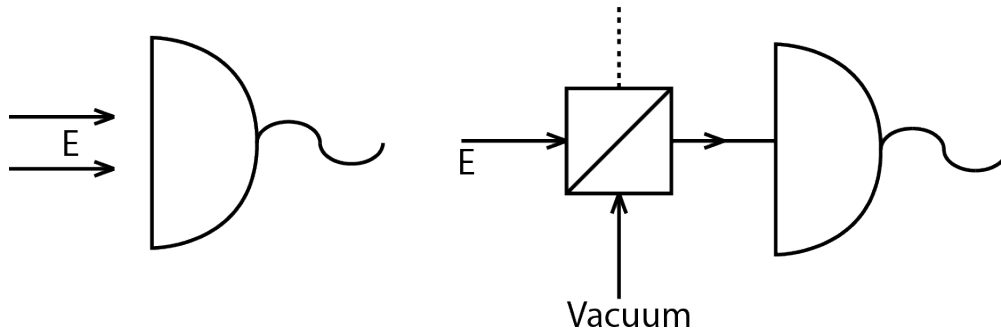


Figure 9: Symbolic image of an ideal photodetector (left) and a realistic photodetector (right).

tively speaking, i.e. not in the single photon regime) field intensities, as this is the relevant case for our experiment. The common characteristic of all such photodetectors is that they produce an output current (photocurrent) proportional to the optical power P (intensity integrated over detector area) of the incident light, i.e.

$$i_{pc} = \eta_{det}|P|,$$

where η_{det} is called the detection efficiency or responsivity of the detector.

An important parameter for such a photodetector is the quantum efficiency η_{QM} , which is the probability that an incident photon is converted to an electric signal and therefore contributes to the photocurrent (possible reasons that an incident photon might not contribute to the photocurrent are that it is not absorbed by the material - i.e. reflected, transmitted or scattered off - or recombination of the electron-hole pair). Assuming that the detector is designed such that every incident photon is converted to exactly one electron contributing to the photocurrent with a quantum efficiency η_{QM} (and doesn't contribute anything otherwise), we can write the proportionality factor between photocurrent and optical power as

$$\eta_{det} = \eta_{QM} \frac{e}{\hbar\omega},$$

where e denotes the charge of one electron. Note that these properties are strictly valid only in the linear dynamic range of the photodetector, outside of this range other effects

(such as saturation) might play an important role and have to be considered.

Typically an electron (or electron-hole pair) generated by the absorption of a photon will contribute to the photocurrent for some average time τ . If changes in the optical power occur on a timescale much larger than τ , we can simply absorb this as an effective gain G in the power-photocurrent relation:

$$i_{pc} = G \eta_{det} |P|.$$

If the gain is only due to τ , we may write

$$G = \frac{\tau}{\tau_o},$$

where τ_o is the transit time of the electron around the electrical circuit (connected to the photodetector).

If the power however changes on a timescale comparable to τ or even τ_o , the simple linear relation between photocurrent and optical power isn't valid. In this case one has to integrate the optical power over a timescale larger than τ to get the right values for the photocurrent, i.e.

$$i(t) = \eta_{det} \int_{-\infty}^t dt' p(t, t') P(t').$$

Here $p(t, t')$ denotes the probability that an electron generated at t' still contributes to the photocurrent at t . For simplification we use

$$i(t) = \eta_{det} \int_{t-T}^t dt' p(t, t') P(t'),$$

where T is large compared to τ but still small compared to timescales we are interested in (it depends on the experimental situation whether such a choice is possible).

The circuit connected to the photodetector is usually designed such that $p(t, t') = 1$, i.e. the current is proportional to the average of the optical power over a time T .

In quantum optical experiments one is often interested in the statistics of the photons rather than their average number (i.e. the intensity or power). To see which of these statistics are still available in the photocurrent after detection we have to change to a quantum mechanical picture. In section 3.1 we have seen that we can define annihilation/destruction operators for a beam such that $a^\dagger a = \frac{P(t)}{\hbar\omega}$. The observable (photocount operator) measured by a photodetector with perfect quantum efficiency can therefore be written as

$$C(t) := \int_{t-T}^t dt' a^\dagger(t') a(t').$$

In the case of a finite quantum efficiency it is not sufficient to just add a prefactor to the preceding equation. As the photons, which do not contribute to the photocurrent, are assumed to be randomly selected, one can however model such a photodetector by adding a beam splitter in front of a perfect photodetector (compare to [8]). The resulting model is graphically shown in figure 9 and the photocount operator can be expressed as

$$C_{real}(t) := \int_{t-T}^t dt' d^\dagger(t') d(t'),$$

where $d := \sqrt{\eta_{QM}} a - \sqrt{1 - \eta_{QM}} v$ and v is the annihilation operator of the vacuum state. The expectation value of course fulfills

$$\langle C_{real}(t) \rangle = \eta_{QM} \langle C(t) \rangle,$$

the variance can be expressed as

$$(\Delta C_{real}(t))^2 = \eta_{QM}^2 (\Delta C(t))^2 + \eta_{QM}(1 - \eta_{QM}) \langle C(t) \rangle.$$

The first term on the right stems from the inherent optical intensity noise and is often called shot noise. The second term is due to the random removal of photons by the beam splitter (non-perfect detector). Note that for a coherent state with time-independent amplitude α (the argument also holds if α is time-dependent, but doesn't change appreciably on a timescale set by T) we have

$$\langle C_{real} \rangle = \eta_{QM} T |\alpha|^2$$

and

$$(\Delta C_{real})^2 = \langle C_{real} \rangle.$$

In addition to the imprinted optical noise there are other current noise sources related to the detector and the detection circuit. Two main noise sources are the dark noise of the detector (i.e. false detection events) and the Johnson noise of the electric circuit. These noise sources can be easily measured (simply by measuring the current without any incident light). Often the photocurrent (or the corresponding voltage) is amplified before the measurement, in which case one has to consider the noise added by the amplifier (which is in general current-dependent).

In our experimental measurement scheme we are shot noise limited (as shown in section 4.2.5).

3.5 Homodyne detection

A normal photodetector (see the preceding section) measures the intensity (or photon number) of light. However, using interferometric methods, it is possible to directly measure the quadratures of the field. The most common methods of doing so are called heterodyne and homodyne detection, their working principle is shown in figure 10. An input beam is combined with a reference beam (local oscillator) at a (usually balanced) beam splitter. The intensities behind the two output ports of the beam splitter are then measured and subtracted from each other. For most applications the intensity of the local oscillator is much stronger than the intensity of the input beam and we are going to assume that in the following calculations. The difference between heterodyne and homodyne detection

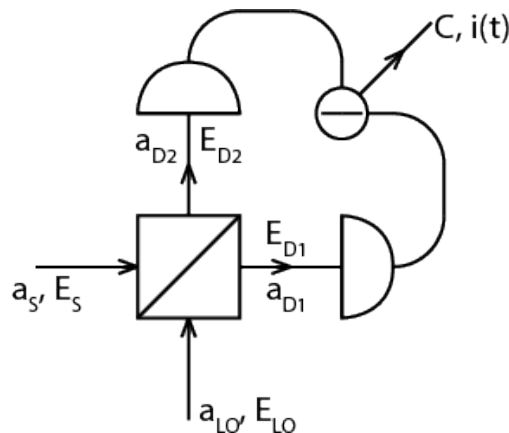


Figure 10: Symbolic setup of heterodyne and homodyne detection.

is that in homodyne detection the reference beam (local oscillator) stems from the same source as the signal beam and therefore has the same wavelength, whereas in heterodyne detection the wavelength of the reference beam might differ from the one of the signal beam. Let us now derive the properties of the measured current, assuming that both signal beam and reference beam can be modeled as plane waves (with noise) with a fixed linear polarization, i.e. we write

$$E_S(t) = (E_S + \delta E_S(t))e^{-i(\omega t - \vec{k}\vec{x})} + (E_S^* + \delta E_S^*(t))e^{i(\omega t - \vec{k}\vec{x})}$$

and

$$E_{LO}(t) = (E_{LO} + \delta E_{LO}(t))e^{-i(\omega t - \vec{k}\vec{x} + \phi(t))} + (E_{LO}^* + \delta E_{LO}^*(t))e^{i(\omega t - \vec{k}\vec{x} + \phi(t))}.$$

Here we have written the electric field amplitudes in terms of their mean amplitude (E_S resp. E_{LO}) and an additional noise amplitude ($\delta E_S(t)$ resp. $\delta E_{LO}(t)$). This classical noise can have different origins usually related to the materials in the propagation path of the beam (e.g. thermal noise of a mirror the beam is reflected off). We will from now on assume that $\text{Arg}(\delta E(t)) \ll 1 \quad \forall t$ is valid for both the signal beam and the local oscillator (if the noise stems from the displacement noise of a mirror, this condition translates to $x_M(t) \ll \lambda \quad \forall t$, where x_M denotes the displacement of the mirror and λ is the electromagnetic wavelength). For simplicity we absorb any unwanted phase difference the beams acquire relative to each other in the parameter $\phi(t)$ and we choose the overall phase such that the mean amplitudes are real. Therefore we can write the power at the detectors as (assuming a balanced beam splitter)

$$\frac{P_{D1}(t)}{\hbar\omega} = \frac{1}{2}(|E_S(t)|^2 + |E_{LO}(t)|^2) - \frac{1}{4}(E_S^*(t)E_{LO}(t) + E_S(t)E_{LO}^*(t))$$

and

$$\frac{P_{D2}(t)}{\hbar\omega} = \frac{1}{2}(|E_S(t)|^2 + |E_{LO}(t)|^2) + \frac{1}{4}(E_S^*(t)E_{LO}(t) + E_S(t)E_{LO}^*(t)).$$

According to the last section we can write the photocurrent (for equal detection efficiencies of the photodetectors) as

$$\begin{aligned} i(t) &\propto P_{D2}(t) - P_{D1}(t) \\ &= E_S E_{LO} \cos(\phi(t)) + E_{LO} [X_S(t) \cos(\phi(t)) + P_S(t) \sin(\phi(t))] \\ &\quad + E_S [X_{LO}(t) \cos(\phi(t)) - P_{LO}(t) \sin(\phi(t))], \end{aligned}$$

where we have neglected terms of second order in the noise amplitudes and the quadratures are defined as

$$X(t) = \frac{1}{2}(\delta E^*(t) + \delta E(t))$$

and

$$P(t) = i\frac{1}{2}(\delta E^*(t) - \delta E(t)).$$

Often this scheme is used to measure the phase quadrature of the input beam, in which case one sets $\phi(t) = \frac{\pi}{2}$ (e.g. by locking the phase below the signal frequency) and $E_S \ll E_{LO}$. Then the current becomes

$$i(t) \propto E_{LO} P_S(t).$$

In the quantum mechanical calculations one has to replace the field amplitudes with the annihilation operator. We choose again the familiar form $a(t) = \alpha(t) + \delta a(t)$ for both signal and local oscillator with $\alpha(t)$ denoting the expectation value of $a(t)$ (the overall phase is chosen such that α is real) and $\delta a(t)$ being the "noise operator". The result is formally the same as in the classical case and we get for the photocount difference operator (making the same approximations as above)

$$\begin{aligned} C^-(t) &:= a_{D2}^\dagger(t)a_{D2}(t) - a_{D1}^\dagger(t)a_{D1}(t) \\ &= \alpha_{LO}(t)P_S(t), \end{aligned}$$

where we have assumed perfect quantum efficiency of the detectors and already set $\phi = \frac{\pi}{2}$. Note that the quadratures are again defined by

$$X(t) = \frac{1}{2}(\delta a^\dagger(t) + \delta a(t))$$

and

$$P(t) = i\frac{1}{2}(\delta a^\dagger(t) - \delta a(t)).$$

The main difference to the classical model in this case is that the beams now have inherent quantum mechanical noise.

The calculations are a little more complicated if one accounts for imperfect detectors (i.e. in the model one adds a beam splitter in front of each detector), the expression for the current operator becomes

$$C_{real}^-(t) := d_{D2}^\dagger(t)d_{D2}(t) - d_{D1}^\dagger(t)d_{D1}(t),$$

where d is defined as in the last section. If both photodetectors have finite, but equal quantum efficiencies η , this leads to the expectation value

$$\langle C_{real}^-(t) \rangle = \eta \langle C^-(t) \rangle$$

and the variance

$$(\Delta C_{real}^-(t))^2 = \eta^2 (\Delta C^-(t))^2 + \eta(\eta - 1) \langle a_S^\dagger(t)a_S(t) + a_{LO}^\dagger(t)a_{LO}(t) \rangle.$$

If it is necessary to account for the finite response time of the detectors, these relations become

$$\begin{aligned} C^- &= \int_{t-T}^t dt' \alpha_{LO}(t') P_S(t'), \\ C_{real}^- &:= \int_{t-T}^t dt' [d_{D2}^\dagger(t')d_{D2}(t') - d_{D1}^\dagger(t')d_{D1}(t')] \end{aligned}$$

and

$$(\Delta C_{real}^-(t))^2 = \eta^2 (\Delta C^-(t))^2 + \eta(1 - \eta) \int_{t-T}^t dt' \langle a_S^\dagger(t)a_S(t) + a_{LO}^\dagger(t)a_{LO}(t) \rangle.$$

In our setup we use homodyne detection to get direct access to the optical phase quadrature. As we will see, coupling of the optical phase to the mechanical position allows us to measure the mechanical quadratures as well.

3.6 Mechanical oscillators and the effective mass

So far in our calculation we have always treated the mechanical oscillator as one-dimensional and with a single resonance frequency. However, the oscillators used in experiments usually behave quite different and usually have many different resonance frequencies (corresponding to different spatial modes) and they obviously aren't one-dimensional. A typical oscillator and one of its mode shapes is shown in figure 11.

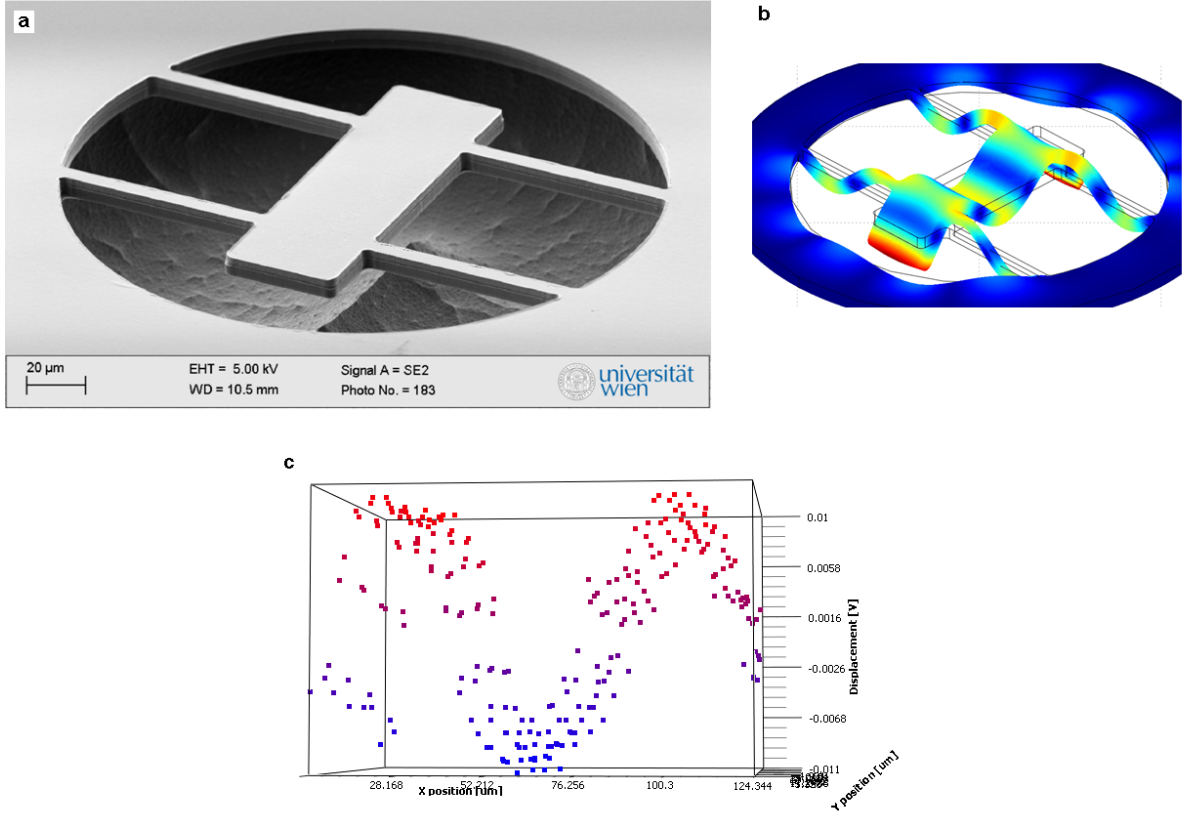


Figure 11: (a) Scanning electron micrograph of the resonator. (b) Predicted 11MHz mode shape using FEM (finite element method). (c) Measured 11MHz mode shape (using optical interferometry).

We therefore need to justify the use of the simple model in our calculations (and, on the way, answer a few remaining questions like "What is the mass that shows up in the calculations?"). The pioneering work in this area has been done by Pinard et. al. ([19],[20]), what I am going to present now is mainly a summary of these results.

We have already remarked multiple times that a cavity, depending on its geometry, will only support certain spatial (transverse) modes. The requirement for some transverse field distribution to be a stable cavity mode is that the distribution will be reproduced after one roundtrip. For a derivation of "usual" cavity modes see e.g. [16]. We will from now on assume that the fundamental mode of the cavity supports a spatial profile $v_0(r) \propto e^{-\left(\frac{r}{w_0}\right)^2}$ (where r denotes the transverse distance from the center, w_0 depends on the cavity geometry and v_0^2 is normalized) and that the incident light is matched to the fundamental mode of the cavity.

We furthermore assume that the displacement⁶ of the moving mirror can be written as a

⁶In this section we denote the displacement by \vec{u} , as x is used for a spatial coordinate. Since we also consider transverse displacements, \vec{u} is a vector quantity.

sum over independent modes, i.e.⁷

$$\vec{u}(t, \vec{x}) = \sum_n \beta_n(t) \vec{u}_n(\vec{x}).$$

Both assumptions are fulfilled for typical optical cavities and mechanical resonators (see e.g. [16], [20]). It can then be shown [19] that each mode amplitude β_n behaves like a one-dimensional harmonic oscillator characterized by the susceptibility

$$\chi_n(\omega) = \frac{1}{m_n(\Omega_n^2 - \omega^2 - i\omega\gamma)}$$

with mass

$$m_n = \rho \int_V dV |\vec{u}_n(\vec{x})|^2, \quad (48)$$

where the integration runs over the volume of the mirror and ρ denotes the density of the mirror (which is assumed to be uniform). We have also assumed that each mode experiences the same damping. Including the thermal forces $F_{T,n}$ (related to the susceptibilities by the fluctuation-dissipation theorem) and the radiation pressure force

$$\vec{F}_{rad}(t, r) = 2\hbar k v_0^2(r) I(t) \vec{e}_x,$$

where the intensity is defined as the rate of photons incident on the mirror, we have

$$\beta_n(\omega) = \chi_n(\omega) \left(2\hbar k I(\omega) \langle u_{n,x} | v_0^2 \rangle + F_{T,n}(\omega) \right).$$

Here we have used

$$\langle u_{n,x} | v_0^2 \rangle := \int dy \int dz u_{n,x}(0, y, z) v_0^2(r).$$

Denoting the mean displacement (averaged over the optical waist) by

$$\bar{u}(t) = \int dy \int dz u_x(0, y, z, t) v_0^2(r),$$

we can write

$$\bar{u}(\omega) = \chi_{eff}(\omega) \left(2\hbar k I(\omega) + F_T(\omega) \right)$$

with

$$\chi_{eff}(\omega) = \sum_n \chi_n(\omega) \langle u_{n,x} | v_0^2 \rangle^2$$

and

$$F_T(\omega) = \frac{1}{\chi_{eff}(\omega)} \sum_n \chi_n(\omega) \langle u_{n,x} | v_0^2 \rangle F_{T,n}(\omega).$$

Since the forces $F_{T,n}$ are related to the susceptibilities χ_n via the fluctuation-dissipation theorem, it follows that F_T is related to χ_{eff} via the fluctuation-dissipation theorem as well.

⁷In Pinard's papers the mechanical amplitudes have been denoted by $a_n(t)$. I changed the notation here to $\beta_n(t)$ to avoid any confusion with the optical annihilation operator.

The mechanical equation of motion for the mirror takes therefore the same form as in the one-dimensional treatment.

Furthermore, assuming small displacements and a high-finesse cavity, the effect (per round trip) of the mirror motion on the field propagating in the cavity is a global phase shift [19]

$$\phi = 2\frac{\omega_L}{c}\bar{u}(t)$$

and the familiar one-dimensional relations follow. If we are primarily interest in one mode, we can define

$$\bar{u}_n(t) = \beta_n(t)\langle u_{n,x}|v_0^2\rangle$$

and get the equation

$$\bar{u}_n(\omega) = \chi_{n,eff}(\omega)\left(2\hbar kI(\omega) + \frac{F_{T,n}(\omega)}{\langle u_{n,x}|v_0^2\rangle}\right)$$

with

$$\chi_{n,eff}(\omega) = \langle u_{n,x}|v_0^2\rangle^2\chi_n(\omega) = \frac{1}{m_{n,eff}(\Omega_n^2 - \omega^2 - i\omega\gamma)},$$

where

$$m_{n,eff} = \frac{m_n}{\langle u_{n,x}|v_0^2\rangle^2}, \tag{49}$$

is called the effective mass of the mode n . Note that

$$\chi_{eff}(\omega) = \sum_n \chi_{n,eff}(\omega)$$

We have seen that we can describe a single mechanical mode (illuminated by a laser beam) with the theory introduced for a one-dimensional mechanical oscillator using an effective mass determined by the geometry and the beam position. In section 4.2.3 we determine the effective mass for the oscillator used in our setup with the help of the above equations.

4 Pulsed quantum optomechanics

While most of the theory of quantum optomechanics reviewed in section 2 did not assume a particular form for the input field, most of the attention so far has gone to the case of a continuous gaussian input field. The study of this interaction has produced a wide range of results (see e.g. reference [13] for a review). The focus on this work however lies on the study of the interaction between a short electromagnetic pulse and a mechanical oscillator (the main idea here is to measure the mechanical position with a precision better than the ground state/thermal state width and thereby achieving squeezing/squashing of the mechanical state). As we will see, this interaction leads to novel results in the field of quantum optomechanics. In addition, since the electromagnetic pulse is very short compared to the mechanical period, the harmonic evolution of the mirror can be neglected, leading to a simple theoretical framework. The first subsection introduces the theory of the pulsed interaction based on the general optomechanical theory in section 2. In the second subsection I will present the specific setup used for the proof-of-concept experiment and the third subsection contains the obtained results.

4.1 Theory

The notation is similar to the one already used in the beginning of this thesis. We will work in the rotating frame and use a_{LO} for the annihilation operator of the reference beam, a_{in} and a_{out} will denote the annihilation operators of the signal beam prior resp. after the interaction with the mirror (cavity). For all optical annihilation operators we consider the division

$$a(t) = \alpha(t) + \delta a(t),$$

where α denotes the expectation value of a and corresponds to the pulse shape. We will furthermore assume that the optical state is a coherent continuous-mode state (i.e. $\alpha(t)$ corresponds to the wavepacket amplitude and $\delta a(t)$ acts on the vacuum state). As already mentioned in section 3.5 we can choose a phase convention s.t. all the α 's are real (assuming small mechanical displacements). The optical quadratures are then defined as

$$X(t) = \frac{1}{2}(\delta a^\dagger(t) + \delta a(t))$$

and

$$P(t) = i\frac{1}{2}(\delta a^\dagger(t) - \delta a(t)).$$

We will also use the observables

$$X = \int dt X(t)$$

and

$$P = \int dt P(t).$$

The statistics of these observables follow directly from the statistics of $X(t)$ and $P(t)$, they will have a Gaussian distribution with $\langle X \rangle = \langle P \rangle = 0$ and $\Delta X = \Delta P = \frac{1}{4}$.

The mechanical annihilation operator is denoted by b and the mechanical quadratures are defined as (note the factor $\frac{1}{2}$ difference to section 1.1.2)

$$X_M(t) = b^\dagger(t) + b(t)$$

and

$$P_M(t) = i(b^\dagger(t) - b(t)).$$

In addition, we define the rotated mechanical quadrature operators as

$$X_M^\phi(t) = X_M(t) \cos(\phi) + P_M(t) \sin\phi.$$

As the interaction between the pulse and the resonator happens on a time scale much shorter than a mechanical period, one can assume that the position of the resonator is approximately constant during the interaction [5] and we simply write X_M to denote the position quadrature operator at the interaction time.

4.1.1 General

We consider the theory of the interaction of a short pulse with a reflecting oscillator, which is not part of a cavity. This is also the case which is relevant for our proof-of-concept experiment, in which we didn't use a cavity for simplicity. The theory including a cavity is treated in the Appendix A.

The theory for this case considerably simplifies compared to the theory of cavity optomechanics. Assuming small mechanical displacements, the annihilation operator (in the rotating frame) corresponding to the reflected beam is given by

$$a_{out}(t) = (1 + i2kx_0X_M)a_{in}(t).$$

or

$$\alpha_{out}(t) = \alpha_{in}(t)$$

and

$$\delta a_{out}(t) = \delta a_{in}(t) + i2kx_0X_M[\alpha_{in}(t) + \delta a_{in}(t)].$$

Here x_0 is defined as in section 1.3.2. The phase detected in the homodyne measurement is then given by

$$P_{out}(t) = 2kx_0X_M[\alpha_{in}(t) + X_{in}(t)] + P_{in}(t)$$

and the measurement operator is again (see section 3.5)

$$P_L = \int_{-\infty}^{\infty} dt \alpha_{LO}(t) P_{out}(t).$$

Assuming a rectangular pulse shape (i.e. small rise/fall time compared to the pulse duration, s.t. $\alpha_{LO}(t) = \alpha_{LO}$ during the pulse duration and $\alpha_{LO}(t) = 0$ otherwise), we have

$$P_L = \alpha_{LO} \int dt P_{out}(t),$$

where the integration now runs over the pulse duration. Note that this condition on the local oscillator pulse shape doesn't limit us in any way in our experiment, as we can simply restrict our measurement to a time frame where $\alpha_{LO}(t) = \alpha_{LO}$ is fulfilled (i.e. not measuring during the pulse rise/fall times). As a matter of fact, the local oscillator beam could in principle also be a continuous wave beam without impacting our scheme in any way.

We now introduce the observables

$$P_{in} = \int dt P_{in}(t)$$

and

$$P_{out} = \int dt P_{out}(t),$$

where the integration runs again over the pulse duration. I.e., in this sense, P_{in} denotes the phase of the pulse prior to the interaction and P_{out} denotes the phase after the interaction. Introducing the coupling parameter

$$\chi = 2kx_0 \int dt \alpha_{in}(t), \quad (50)$$

we obtain for the measured observable

$$P_L = \alpha_{LO} P_{out} = \alpha_{LO} (\chi X_M + P_{in}). \quad (51)$$

Here we have neglected the term proportional to $X_M \int dt X_{in}(t)$. This leads to an expectation value

$$\langle P_L \rangle = \alpha_{LO} \chi \langle X_M \rangle$$

and (since X_M and P_{in} are uncorrelated) to a variance

$$(\Delta P_L)^2 = \alpha_{LO}^2 \left(\chi^2 (\Delta X_M)^2 + (\Delta P_{in})^2 \right).$$

For non-perfect photodetectors (assuming both photodetectors have finite quantum efficiency η) the variance becomes

$$\begin{aligned} (\Delta P_L)^2 &= \eta^2 \alpha_{LO}^2 \left(\chi^2 (\Delta X_M)^2 + (\Delta P_{in})^2 \right) + \eta(1-\eta)(N_S + N_{LO}) \\ &\approx \eta \alpha_{LO}^2 \left(\eta \chi^2 (\Delta X_M)^2 + \eta (\Delta P_{in})^2 + (1-\eta)T \right), \end{aligned}$$

where we have introduced the notation $N_{LO} = \int dt \alpha_{LO}^2(t) = T \alpha_{LO}^2$ (where T denotes the pulse duration or measurement time) and $N_S = \int dt \alpha_{in}^2(t)$ for the mean photon numbers of the local oscillator and signal pulse. Note that in the last line we have assumed that $N_S \ll N_{LO}$. As the pulse duration is very short, the last term on the right is usually negligible and we obtain the same results as in the case of perfect photodetectors (with the local oscillator amplitude scaled by η).

4.1.2 State preparation

Equation 51 tells us that the pulsed measurement can be seen as a position measurement of the mechanical oscillator with the measurement uncertainty determined by the

optical phase distribution (and, in particular, a rms measurement error of $\frac{1}{\chi}\Delta P_{in}$). Therefore, following the discussion of quantum measurements provided in section 2.2, given a measurement outcome p_L , the resulting mechanical state immediately after the measurement (assuming the mechanical probability distribution of the initial state doesn't change appreciably on a scale $\frac{\Delta P_{in}}{\chi}$) has a Gaussian distribution with expectation value

$$\langle X_M \rangle \approx \frac{p_L}{\alpha_{LO} \chi}$$

and variance

$$(\Delta X_M)^2 \approx \frac{1}{\chi^2} (\Delta P_{in})^2.$$

The mechanical evolution during the measurement (neglecting harmonic evolution, i.e. just momentum transfer) is formally determined by

$$\dot{b} = i f_0 a_{in}^\dagger a_{in}$$

with $f_0 = 2kx_0$ and describes the momentum transfer to the mechanical oscillator. The observable corresponding to the transferred momentum is thus

$$M = 2f_0 \int dt a_{in}^\dagger a_{in} \approx 2f_0 \left(\int dt \alpha_{in}(t)^2 + 2 \int dt \alpha_{in}(t) X_{in}(t) \right)$$

so the mean momentum transferred per pulse is

$$\bar{M} = 4kx_0 N_S,$$

and the uncertainty is

$$\Delta M \approx 4\chi \Delta X_{in}. \quad (52)$$

Note that the uncertainty relation is fulfilled, i.e.

$$\Delta X_M \Delta M \approx 4\Delta X_{in} \Delta P_{in} = 1.$$

The factor is due to the different choice of units for the optical and mechanical quadratures (i.e. for the optical quadratures the uncertainty relation reads $\Delta X \Delta P = \frac{1}{4}$ and for the mechanical quadratures it reads $\Delta X_M \Delta P_M = 1$).

We will now give a more detailed treatment and apply the theory of section 2.2 to determine the mechanical state after the evolution. The propagator U determining the output state via $P_{out} = U P_{in} U^\dagger = P_{in} + \chi X_M$ (and $X_{out} = U X_{in} U^\dagger = X_{in}$) as well as $P_{M,out} = U P_{M,in} U^\dagger = P_{M,in} + M$ (and $X_{M,out} = U X_{M,in} U^\dagger = X_{M,in}$) is given by

$$U = e^{i\frac{\bar{M}}{2} X_M} e^{i2\chi X_M X_{in}},$$

as can be easily seen by noting that $[P_{in}, X_{in}^n] = -i\frac{n}{2} X_{in}^{n-1}$ and $[P_{M,in}, X_{M,in}^n] = -i2n X_{M,in}^{n-1}$. We will from now on denote the (formal) eigenstates of the optical observable P (P_{in} , P_{out}) with $|p\rangle$.

Let us now switch to the Schroedinger picture and assume for a moment the mechanical state is a pure state $|\varphi_{in}\rangle$. Then, acting on the wave function (note that in the optical

p -representation $X_{in} = i\frac{1}{2}\frac{\partial}{\partial p}$ due to our choice of units and the optical wave function is simply the vacuum state), we obtain

$$\langle p, q|U|\psi_{in}, \varphi_{in}\rangle = \left(\frac{\pi}{2}\right)^{-\frac{1}{4}} e^{i\frac{1}{2}\bar{M}q} e^{-(p-\chi q)^2} \varphi_{in}(q),$$

i.e. in the notation of section 2.2.2 we have

$$\beta(q, q'; \tilde{p}) = \left(\frac{\pi}{2}\right)^{-\frac{1}{4}} \delta(q - q') e^{i\frac{1}{2}\bar{M}q} e^{-(\tilde{p}-\chi q)^2}$$

and

$$\Omega(\tilde{p}) = \left(\frac{\pi}{2}\right)^{-\frac{1}{4}} e^{i\frac{1}{2}\bar{M}X_M} e^{-(\tilde{p}-\chi X_M)^2}.$$

This operator determines the output state via

$$|\varphi_{out}\rangle = \frac{1}{\sqrt{w(\tilde{p})}} \Omega(\tilde{p}) |\varphi_{in}\rangle,$$

where

$$w(\tilde{p}) = \left(\frac{\pi}{2}\right)^{-\frac{1}{2}} \int dq |\varphi_{in}(q)|^2 e^{-2(\tilde{p}-\chi q)^2}. \quad (53)$$

is the probability distribution of measurement outcomes. Note that $\Omega(\tilde{p})$ has a straightforward interpretation, the first factor produces the momentum transfer via

$$e^{i\frac{1}{2}\bar{M}X_M} |p_M\rangle = |p_M - \bar{M}\rangle$$

(note that $X_M = i2\frac{\partial}{\partial p_M}$ in the mechanical momentum representation) and the second factor narrows the mechanical position probability distribution to a width scaling with $\frac{1}{\chi^2}$. If the initial mechanical state is in a mixed state described by a density matrix ρ_{in} the output state is determined by

$$\rho_{out} = \frac{1}{w(\tilde{p})} \Omega(\tilde{p}) \rho_{in} \Omega^\dagger(\tilde{p})$$

with

$$w(\tilde{p}) = \left(\frac{\pi}{2}\right)^{-\frac{1}{2}} \int dq \langle q|\rho_{in}|q\rangle e^{-2(\tilde{p}-\chi q)^2}.$$

Note that here \tilde{p} refers to the phase (i.e. a measurement of the observable P_{out}), which is measured via homodyne detection as described above (i.e. $\tilde{p} = \frac{p_L}{\alpha_{LO}}$). In terms of the measurement outcome p_L the resulting mechanical state is thus

$$\rho_{out}(p_L) = \frac{1}{w(\frac{p_L}{\alpha_{LO}})} \Omega\left(\frac{p_L}{\alpha_{LO}}\right) \rho_{in} \Omega^\dagger\left(\frac{p_L}{\alpha_{LO}}\right)$$

If the initial mechanical state is a thermal state with large mean occupation \bar{n} , we have already seen that the state after the first pulse with measurement outcome $p_{L,1}$ has a Gaussian position distribution with mean proportional to $\frac{p_{L,1}}{\chi\alpha_{LO}}$ and variance $\frac{1}{4\chi^2}$. Note that the variance in momentum space after the pulse is given by $(\Delta P_M)^2 + (\Delta M)^2$, where $(\Delta P_M)^2 = 2\bar{n} + 1$ is the initial momentum variance of the thermal state as given in equation

45 and $(\Delta M)^2 = 4\chi^2$ is the uncertainty in the transferred momentum as given in equation 52. We therefore obtain for the rotated quadratures

$$\langle X_M^\Theta \rangle = \frac{p_{L,1}}{\alpha_{LO} \chi} \cos(\Theta) - \bar{M} \sin(\Theta) \quad (54)$$

and

$$(\Delta X_M^\Theta)^2 = \frac{1}{4\chi^2} \cos^2(\Theta) + (1 + 2\bar{n} + 4\chi^2) \sin^2(\Theta). \quad (55)$$

A full derivation of these results (for an arbitrary initial occupation of the thermal state) by calculating $\Omega(\frac{p_L}{\alpha_{LO}}) \rho_{th} \Omega^\dagger(\frac{p_L}{\alpha_{LO}})$ (where ρ_{th} denotes the density matrix of the thermal state as given in 43) can be found in [5].

The resulting state after the pulsed interaction has therefore a reduced uncertainty in

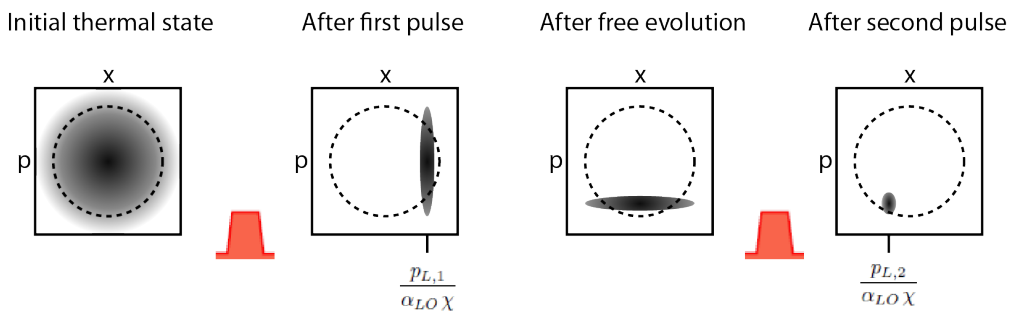


Figure 12: Schematic phase-space representation of the measurement scheme utilizing two pulses. The gray area corresponds to the Wigner function of the mechanical state.

the position quadrature but the uncertainty in the momentum quadrature has not been changed (assuming $\chi \ll \bar{n}$). We can achieve a reduced uncertainty in both quadratures by utilizing a second pulse after the oscillator has evolved harmonically for a quarter period and the initial momentum uncertainty has turned in position uncertainty (see figure). Denoting the outcome of the second pulse as $p_{L,2}$, we find for the resulting state

$$\langle X_M^\Theta \rangle = \frac{p_{L,2}}{\alpha_{LO} \chi} \cos(\Theta) - \bar{M} \sin(\Theta) \quad (56)$$

and

$$(\Delta X_M^\Theta)^2 \approx \frac{1}{4\chi^2} \cos^2(\Theta) + (\frac{1}{4\chi^2} + 4\chi^2) \sin^2(\Theta). \quad (57)$$

To quantify the purity of the resulting state we define an effective mechanical occupation via

$$1 + 2\bar{n}_{eff} = \Delta X_M^0 \Delta X_M^{\frac{\pi}{2}}.$$

We can furthermore define an effective temperature in analogy to equation 46, i.e. by

$$T_{eff} = \frac{\hbar\omega_M}{k_B} (\bar{n}_{eff} + \frac{1}{2}). \quad (58)$$

We will use this effective temperature in section 4.3 to compare the states after the pulsed interaction to the initial thermal states.

4.1.3 State reconstruction

To quantify the mechanical state after it has been prepared with a pulse as described above, we have to measure the rotated quadrature probability distributions as described in section 2.1.

For this we can simply utilize a second pulse after the mechanical oscillator has evolved by an angle $\Theta = \omega_M t$. If the first pulse with measurement outcome $p_{L,1}$ has prepared the oscillator in a state $\rho(p_{L,1})$, the state after this harmonic evolution is given by $e^{-i\Theta b^\dagger b} \rho(p_{L,1}) e^{-i\Theta b^\dagger b}$ and the probability distribution of the measurement outcomes for the second pulse is given by

$$w(p_{L,2}) = \left(\frac{\pi}{2}\right)^{-\frac{1}{2}} \int dq \langle q | e^{-i\Theta b^\dagger b} \rho(p_{L,1}) e^{-i\Theta b^\dagger b} | q \rangle e^{-2\left(\frac{p_{L,2}}{\alpha_{LO}} - \chi q\right)^2}.$$

Assuming again that the mechanical probability distribution doesn't contain any sharp features (compared to the optical ground state width, i.e. on a scale $\frac{1}{2\chi}$) we can approximate the mechanical position by the measurement outcomes $\frac{p_{L,2}}{\alpha_{LO} \chi}$ and therefore we have access to all mechanical quadratures.

However, the mechanical state after the first pulse has a mean value $\frac{p_{L,1}}{\alpha_{LO} \chi}$, which has to be considered in the analysis. One possibility is to post-select the data (i.e. to only use measurement outcomes $p_{L,2}$ for which the outcomes $p_{L,1}$ were in a narrow window). Another possibility, which was used in our experiment, is to simply subtract the mean (taking the harmonic evolution into account), i.e. to transform the second measurement outcome as

$$p_{L,2} \rightarrow p_{L,2} - p_{L,1} \cos(\Theta).$$

The same measurement protocol can obviously also be applied if the initial mechanical state was prepared by two pulses as described in the last section. In this case the measurement outcome has to be transformed as

$$p_{L,3} \rightarrow p_{L,3} - p_{L,2} \cos(\Theta) + p_{L,1} \sin(\Theta),$$

where $p_{L,1}$ and $p_{L,2}$ are the measurement outcome of the first and second pulse, respectively.

4.2 Proof-of-concept Experiment

We prepared an experimental setup as outlined below to verify the feasibility of our measurement scheme. The aim here was not to obtain a high measurement strength χ , but rather to construct a simply working setup which can then provide a solid basis for future experiments.

4.2.1 Setup

The setup of our experiment is schematically depicted in figure 13a. A single mode laser with an optical wavelength of 1064nm was used as light source, the beam is coupled into a single mode optical fiber and the pulses were then generated from the cw beam by electro-optic amplitude modulation. The pulses are split at an adjustable beam splitter into an intense pulse (local oscillator) and a weaker pulse (signal beam). The ratio of the powers of the two beams was adjusted to approximately 1:100, s.t. the approximations

used in section 3.5 can be applied. The polarization of the signal pulse is adjusted to a linear polarization (from now on referred to as horizontal polarization) with the help of a fiber polarization controller and is, after passing a polarizing beam splitter and a quarter wave plate, focused on and reflected of a micro-mechanical oscillator (shown in figure 13b). The phase of the reflected pulse will therefore depend on the position of the mirror and, for small mirror displacements, can be interpreted as a change in solely the phase quadrature. The reflected pulse has vertical polarization after passing the quarter wave plate and is therefore reflected at the polarizing beam splitter. After this it is recombined with the local oscillator (the polarization of the local oscillator is matched to the signal beam by a fiber polarization controller and its phase is adjusted such that the mean phase is $\frac{\pi}{2}$) at a balanced beam splitter and a homodyne measurement is performed. A typical output signal is shown in figure 13c. The measured quantity is the area under each pulse and the corresponding observable is denoted by P_L .

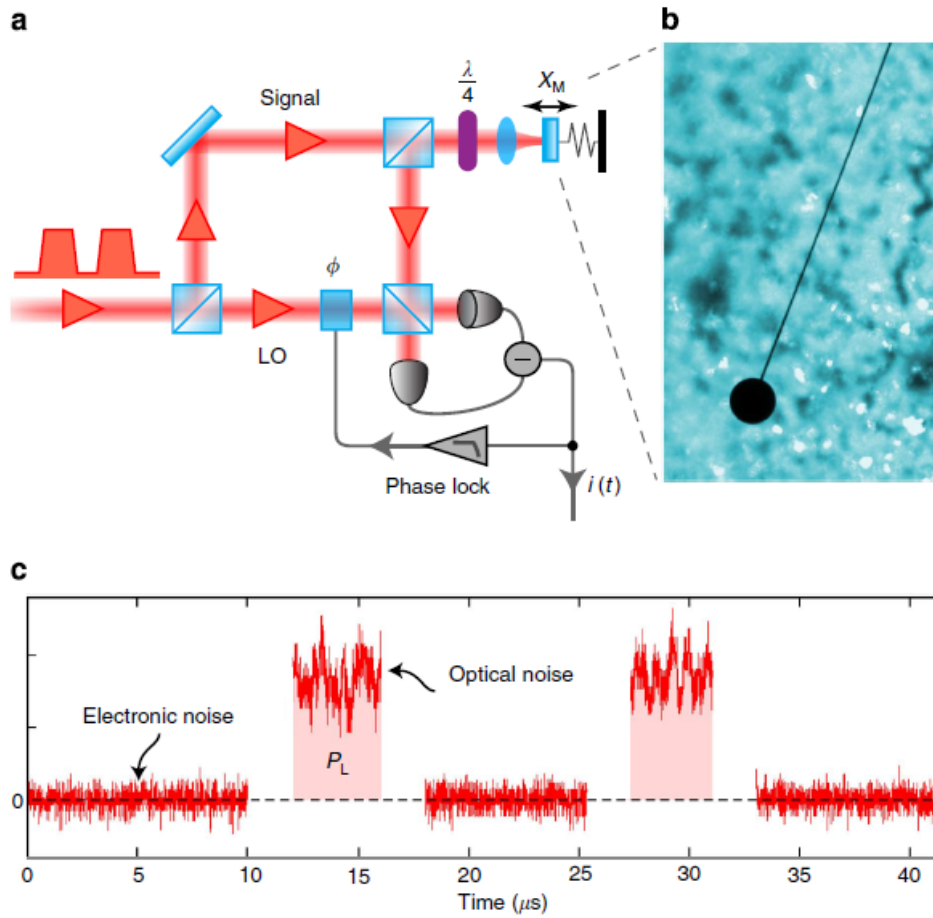


Figure 13: (a) Schematic setup of the experiment. (b) Colourized optical micrograph of mirror used for the experiment. (c) Example time trace of the signal recorded with homodyne detection. The measurement outcome corresponding to P_L is the area under the pulses, not including the rise and fall times.

Figure reprinted from [21].

The reason for not using a cavity in this setup was solely simplicity. This setup was meant as a proof-of-concept experiment and a cavity isn't necessary to proof the feasibility of our scheme⁸. The effect of the cavity is an enhancement of the coupling between the pulse and the mirror (i.e. a stronger shift in the phase of the pulse and more momentum

⁸At the time of the writing of this thesis, the experiment is continued and modified to include a cavity.

transferred to the mirror). On average, both the phase shift and the momentum transfer will be enhanced by a factor corresponding to the times a photon "bounces" back and forth in the cavity. The exact theory including a cavity is presented in appendix A.

4.2.2 Measurement

We performed both the two and the three pulse measurement scheme as detailed in section 4.1.2. For the two pulse scheme, denoting the measurement results of the two pulses with $p_{L,1}$ and $p_{L,2}$ (and $\Theta = \omega_M t$ is the angle of evolution between the first and second pulse), we calculated the quantity $p_L = p_{L,2} - p_{L,1} \cos(\Theta)$ to obtain the final measurement result.

For the three pulse scheme, denoting the measurement outcomes of the three pulses with $p_{L,1}$, $p_{L,2}$ and $p_{L,3}$, respectively (and $\Theta = \omega_M t$ is the angle of evolution between the second and third pulse), we calculated the quantity $p_L = p_{L,3} - p_{L,2} \cos(\Theta) + p_{L,1} \sin(\Theta)$ to obtain the final measurement result.

These values were then binned (see figure 17(b-c) for the resulting distributions) and the Wigner function was then numerically reconstructed as outlined in section 2.1. All measurement results are presented in section 4.3.

4.2.3 The mechanical oscillator

We used a micro-mechanical mirror etched from an $6.88\mu\text{m}$ thick epitaxial $\text{Al}_x\text{Ga}_{1-x}\text{As}$ crystalline multilayer, which exhibits significantly less mechanical damping compared to conventional mirrors with dielectric optical coating but still provides excellent optical reflectivity (uniform 99.982% intensity reflectivity). The cantilever is in total 1.55mm long, with a head of $100\mu\text{m}$ diameter connected to a $5\mu\text{m}$ thick (and 1.45mm long) arm, which in turn is connected to the substrate (see figure 14b). Its fundamental out-of-plane (as the cantilever is slightly thicker than wide, the lowest-frequency mode is an in-plane mode) vibrational mode has a resonance frequency of 984.3Hz .

The mode shape was determined by finite-element analysis of the resonator (see fig-

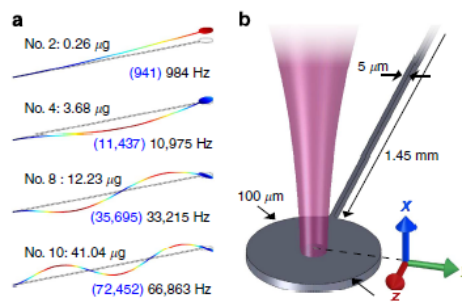


Figure 14: (a)FEM simulation of the four out-of-plane modes with the four lowest optically proved effective masses. The simulated frequencies (in brackets) differ slightly from the measured ones. (b)Schematic of the mechanical resonator and the focused signal beam.

Figure reprinted from [21].

ure 14a) and the effective mass was then calculated with the help of equations 48 and 49, giving an value $m_{eff} = 260\text{ng}$ (for the beam centered on the mirror head). The ground state with is thus given by $x_0 = 5.7 \cdot 10^{-15}\text{m}$. The quality factor was measured in vacuum (10^{-5}mbar) at room temperature via a ring-down measurement and found to be $Q = 3.1 \cdot 10^4$.

The contribution from other out-of-plane modes is already small simply due to the geometry of the mirror (the unconditional RMS amplitudes of modes 4, 8 and 10 are 2.4%, 0.4% and 0.1% that of the fundamental out-of-plane mode, respectively) but can be even further suppressed by careful alignment of the beam at the center of the mirror head (corresponding to a much higher effective mass for these modes, compare to figure 14a). For more information see e.g. [21], [22], [23].

4.2.4 Calibration

The calibration (i.e. the determination of the proportionality between a pulsed measurement outcome and the mechanical position) is done in two steps. In the first step we use a cw beam to determine the proportionality between the voltage applied to the piezo and the displacement of the piezo. For this we focus the beam on a rigid mirror (we used an edge of the chip which also contained the resonator) attached to the piezo and record the homodyne measurement outcome, which is (for arbitrarily large displacements x) given by

$$i(t) \propto \cos\left(\phi - \frac{4\pi}{\lambda}x(t)\right)$$

where ϕ is random (due to the large displacements locking wasn't possible) but approximately constant over a few mechanical periods. This enables us to exactly determine when the peak-to-peak displacement equals half the optical wavelength, which gives us the ratio of driving voltage to piezo displacement (see figure 15). We also verified that response of the piezo to the driving voltage was indeed linear.

In the second step we record the outcome of pulsed measurements for a given driving voltage (and therefore known displacements) chosen such that $x(t) \ll \lambda$ is fulfilled.

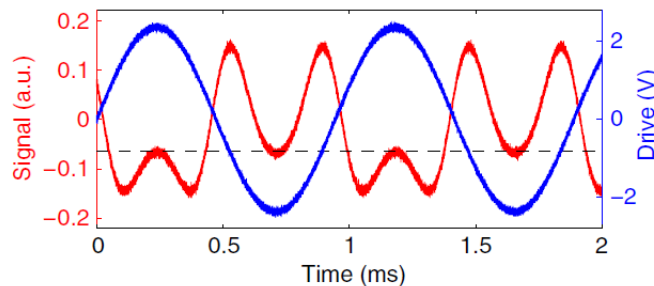


Figure 15: Plot of the homodyne output (red, left axis) while a drive voltage (blue, right axis) is applied to the piezo. The drive voltage corresponds to half an optical wavelength, as can be seen by the coinciding turning points of the homodyne signal (dashed line).

Figure reprinted from [21].

4.2.5 Verification of the shot noise limit

To verify that our measurement scheme is indeed quantum noise limited, we focused the beam on a rigid mirror (as in the calibration procedure) to avoid any coupling to mechanical motion, then we step-wise increased the total optical power (i.e. $N_{Tot} = N_S + N_{LO}$, where the ratio $\frac{N_S}{N_{LO}}$ was kept fixed) and measured the conditional variance of two optical pulses (i.e. we subtracted the measurement outcomes of the two pulses and recorded the resulting value) separated by $14\mu s$ (with a pulse width of $4\mu s$). The quantum noise

of the pulses is uncorrelated and therefore remains in the conditional variance. Any classical noise components would be expected to increase quadratically with optical power [9], whereas quantum noise increases linearly with the optical power. The results of the measurement (figure 16) clearly show the linear dependence of the conditional variance on the optical power. Note that the reason for being quantum limited here is not the ab-

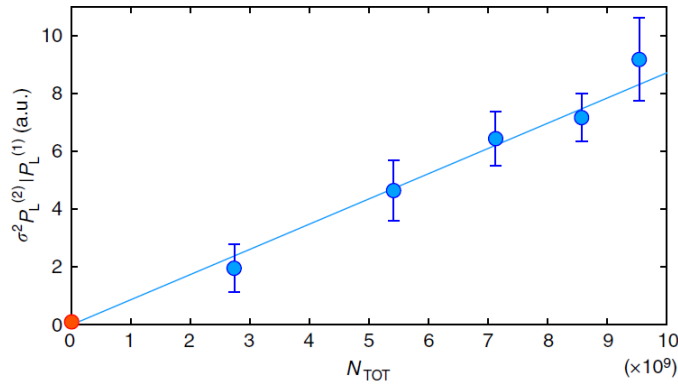


Figure 16: Conditional phase quadrature variance as a function of the total optical power. The linear dependence confirms that the measurement scheme is shot noise limited. Figure reprinted from [21].

sence of classical phase noise between the pulses, but rather that this classical noise is low in frequency and therefore stays correlated over the pulse separation used here. By increasing the pulse separation we lose the linear dependence due to the phase noise, this also limits us in our three-pulse scheme as described in the next section. Note that the pulse separation used here ($14.1\mu s$) corresponds to 5° of mechanical evolution for our harmonic oscillator.

4.2.6 Coupling to a thermal environment

After the oscillator has been prepared in a state with reduced uncertainty (compared to the initial thermal state), coupling with the environment (mechanical clamping, gas molecules, etc..) will increase the uncertainty again until the oscillator's initial thermal state has been restored. For our two- and three-pulse state preparation protocols, we need this rethermalization to be negligible over one mechanical period.

One can model rethermalization of a quantum harmonic oscillator by linear coupling to a bath of harmonic oscillators. This leads to the usual rethermalization rate $\Gamma = \gamma \bar{n}$ (see e.g. [5]). As $\gamma \approx 0.2s^{-1}$ in our setup and the mechanical period is roughly a millisecond, rethermalization over the course of one mechanical period is completely negligible (for the squashed thermal states - if one wants to prepare & characterize quantum states, it's a different story).

4.3 Results

All measurement results are summarized in figure 17. We prepared the mechanical oscillator in a thermal state with $\sigma_x = x_0 \Delta X_M = 1.2nm$ (corresponding to an effective temperature of $T_{eff} = \frac{m_{eff}\omega_M^2}{k_B}\sigma_x^2 \approx 1100K$) by driving with white noise and then characterized this state via pulsed tomography (figure 17a).

We then implemented the two- and three-pulse protocols as described above to both prepare and characterize mechanical states with reduced quadrature uncertainties (figure

17b-c). Note that for the three pulse protocols the uncertainty should not vary with the mechanical evolution angle Θ (but should be roughly $\frac{1}{4\chi^2}$, as demonstrated by equation 57). The reason that it does vary here is that the correlation between the pulses reduces with increasing separation due to low frequency phase noise (caused by the imperfect lock) as described shortly in the last section.

The effective temperature (which is now defined as in equation 58) for this state,

$$T_{eff} = 16K,$$

is therefore due to the classical optical noise and does not accurately describe the mechanical state. Were the pulses to remain quantum noise limited for all Θ , the effective temperature corresponding to our measurement strength would be roughly (also neglecting mechanical thermalization, i.e. simply taking $(\Delta X_M^\Theta)^2 = (\Delta X_M^0)^2 \forall \Theta$) given by

$$T_{eff} \approx 4K.$$

For both the two-pulse scheme and the three-pulse scheme we used the same optical power and each histogram was constructed using 300 measurement outcomes. In figure 17e we summarized the standard deviation of the probability distributions for each of the states described above.

Figure 17d shows a reconstructed driven, thermal state as an example of a non-Gaussian state. This state was generated by sinusoidally driving the piezo at the eigenfrequency of our mechanical oscillator. Note that, as this state was prepared without a white noise drive, the two peaks in its marginals are narrower than the marginals of the thermal state shown in 17a.

The rippling one can observe in the reconstructed Wigner functions is due to the missing read-out pulse for $\Theta = 0$ and could be reduced by using shorter pulses and measuring marginals for smaller Θ .

The scaling of our measurement strength is demonstrated in figure 17f, where we plotted the mechanical position width (standard deviation) as a function of the integrated signal pulse amplitude $\sqrt{2} \int dt \alpha_{in}(t)$, which was determined through a separate power measurement. In slight abuse of notation we use $\sqrt{N} := \sqrt{2} \int dt \alpha_{in}(t)$.

One pulse was used to prepare the state and another pulse, separated from the first one by 5° of mechanical evolution, was used to measure the position. From equation 50 and 55 it follows, that the dependence should be given by

$$\Delta X_M \propto \frac{1}{\sqrt{N}},$$

which is indeed the dependence we have obtained in the experiment. For the largest optical pulse strength the width of the mechanical state was $\sigma_x = 19pm$, corresponding to a measurement strength of

$$\chi \approx 1.51 \cdot 10^{-4}$$

This agrees with the theoretical value $\chi \approx 1.53 \cdot 10^{-4}$, which was calculated using equation 50.

Note that in [21] due to the different definition of the quadratures the obtained measurement strength differs by a factor of $\sqrt{2}$, i.e. there $\chi = 2.1 \cdot 10^{-4}$.

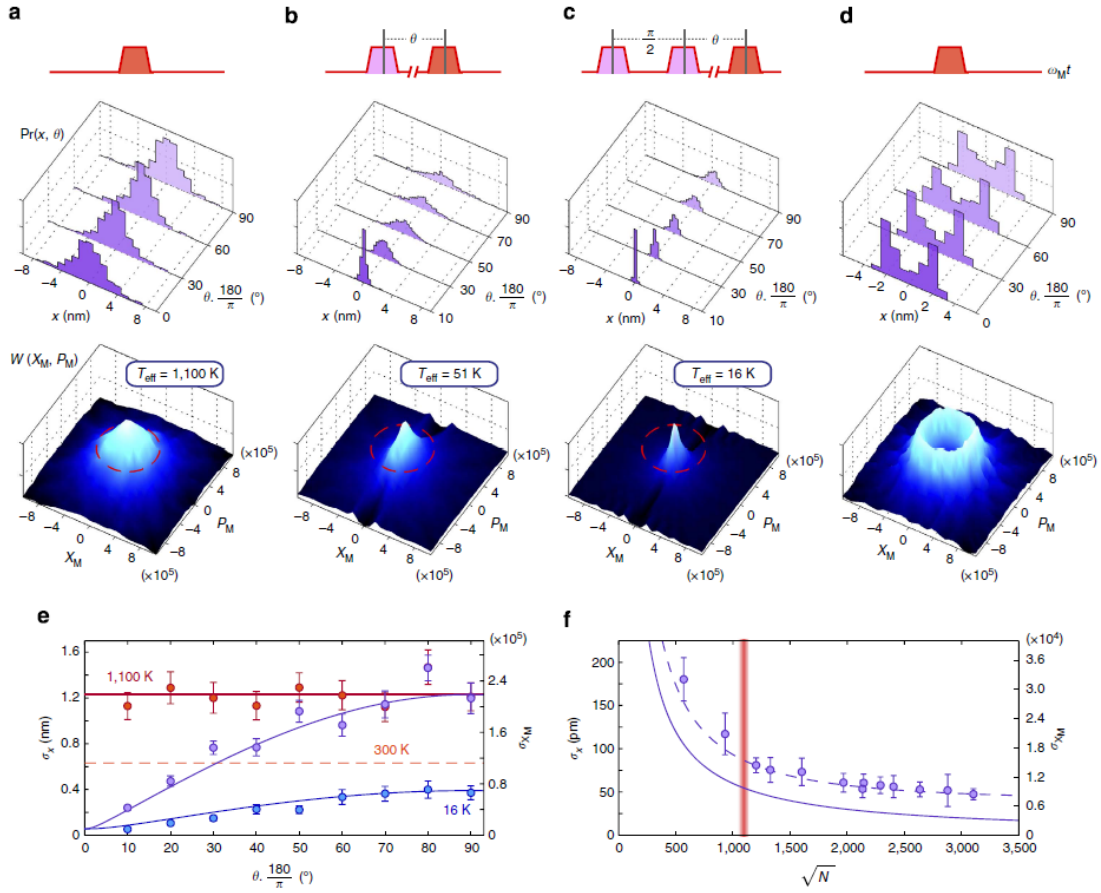


Figure 17: The uppermost row shows the pulse protocols (pink - preparation, red - tomography). The two rows below show a subset of the measured probability distributions of the mechanical quadratures X_M^Θ and the reconstructed Wigner functions, respectively. The phase-space distributions were reconstructed using nine marginal angles up to $\frac{180}{\pi}\Theta = 90^\circ$ (with a larger number of bins used than shown for the distributions in this figure). For our current measurement strength, that is, $\chi \ll 1$, all the mechanical states reconstructed here can be described classically.

(a) In the first column, tomography and reconstruction of an initial mechanical thermal state driven by white noise up to a mode temperature of 1100 K is shown. The red dashed circle has a radius equal to the width of the initial thermal distribution.

(b) A single pulsed measurement reduces the mechanical position variance, but leaves the momentum distribution unchanged.

(c) 'Cooling-by-measurement' performed with two pulses separated by one quarter of a mechanical period rapidly reduces the mechanical state's entropy. The effective temperature of the mechanical state reconstructed here has been reduced to 16 K .

(d) State reconstruction of a non-Gaussian mechanical state of motion generated by resonant sinusoidal drive.

(e) The (one s.d.) width of the position distribution observed for states (a-c) with phase-space angle Θ . The thermal state (red points) shows a position width approximately twice of that when at room temperature (dashed line). State (b) has a reduced position width for small phase-space angles (purple points). The position width of state (c) is reduced for all phase-space angles (blue points). The solid lines are theoretical fits obtained using equation 55 (with χ and \bar{n} as fitting parameters).

(f) Plot of the conditional mechanical width versus pulse strength obtained using two pulses separated by 5° of mechanical evolution. The dashed line is a theoretical fit with a model using two units of optical quantum noise and finite mechanical evolution. The solid line is the inferred conditional mechanical width immediately after the preparation pulse. The vertical line indicates the pulse strength used for states (a-c). The error bars on (e) and (f) indicate a one s.d. uncertainty.

Figure reprinted from [21].

5 Discussion & Outlook

In this work we were able to show preparation of mechanical states of motion by measurements of the mechanical position utilizing short optical pulses. Specifically, starting with an initial thermal state, we have prepared squashed thermal states with a greatly reduced effective temperature (from initially $1100K$ to $16K$). While all of the states we managed to prepare during the duration of this thesis can be fully described by classical physics, I am confident that the methods introduced here will soon lead to the preparation of mechanical quantum states like the squeezed coherent state. I want to highlight once more that (in contrast to any other methods known to the author) this quantum state preparation does not require any additional cooling and can in principle be performed at room temperature.

In addition to state preparation we were also able to characterize the resulting state using pulsed measurements. Again, while all of the reconstructed states were classical, our measurement scheme can be used for quantum state tomography as well. This is due to the quantum-non-demolition nature of our measurement that allows us to overcome the standard quantum limit. For a large measurement strength χ one could, using our method, easily resolve quantum mechanical features smaller than the mechanical ground state.

The setup we have prepared is a good basis for future experiments using pulsed optomechanics. The future challenge will be to enhance the measurement strength χ to a level where quantum mechanical states can be prepared and characterized (which requires $\chi \geq 1$). One way to do this is to use an optical cavity, which must have both a high finesse (using otherwise the experimental parameters achieved in this work, a finesse of 10^4 would be sufficient) and a large bandwidth (to accommodate an optical pulse). Both of these requirements can be met by optomechanical microcavities.

Future applications of our methods are manifold. Concrete examples include the proposal by Buchmann et. al. [25], who considers pulsed measurements, as realized in this work, to observe quantum tunneling of a mechanical oscillator in a double well potential, or the proposal by Sekatski et. al. [26] for the generation of macroscopic quantum superposition states.

It might even be possible to use our scheme for probing quantum-gravitational phenomena experimentally, as has been proposed by Pikovsky et.al. [27].

In conclusion, we have successfully built a proof-of-concept setup for mechanical state preparation via measurement and thereby contributed novel results to the field of quantum optomechanics. Our setup might be improved upon and used for various applications, some of which have been stated above. It is the authors expectation, that it will soon be possible to both prepare and read-out features of macroscopic quantum states with the methods introduced here.

References

- [1] A. D. O'Connell et. al.
Quantum ground state and single-phonon control of a mechanical resonator
Nature 464, 697 (2010)
- [2] J. Chan, T. P. Mayer Alegre, A. H. Safavi-Naeini, J. T. Hill, A. Krause, S. Gröblacher, M. Aspelmeyer & O. Painter
Quantum ground state and single-phonon control of a mechanical resonator
Nature 478, 89 (2011)
- [3] J. D. Teufel et. al.
Sideband cooling of micromechanical motion to the quantum ground state
Nature 475, 359 (2011)
- [4] M. R. Vanner et. al.
Entangling Mechanical Motion with Microwave Fields
Science 342, 710 (2013)
- [5] M. R. Vanner et. al.
Pulsed quantum optomechanics
PNAS 108 (39), 16182 (2011)
- [6] John David Jackson
Classical Electrodynamics
John Wiley & Sons, Inc.
- [7] Braginsky V.B., Khalili F.Ya.
Quantum Measurement
Cambridge University Press
- [8] Rodney Loudon
The Quantum Theory of Light
Oxford Science Publications
- [9] Hans-A. Bachor, Timothy C. Ralph
A Guide to Experiments in Quantum Optics
Wiley-VCH
- [10] C. K. Law
Interaction between a moving mirror and radiation pressure: A Hamiltonian formulation
Phys. Rev. A 51, 2537 (1995)
- [11] C. A. Schrama, D. Bouwmeester, G. Nienhuis, J.P. Woerdman
Mode dynamics in optical cavities
Phys. Rev. A 51, 641 (1995)

- [12] Walter Heitler
The Quantum Theory of Radiation
Oxford University Press
- [13] Markus Aspelmeyer, Tobias J. Kippenberg, Florian Marquardt
Cavity optomechanics
Rev. Mod. Phys. 86, 1391 (2014)
- [14] E. Wigner
On the Quantum Correction For Thermodynamic Equilibrium
Phys. Rev. 40, 749 (1932)
- [15] K. Vogel and H. Risken
Determination of quasiprobability distributions in terms of probability distributions for the rotated quadrature phase
Phys. Rev. A 40, 2847 (1989)
- [16] Anthony E. Siegman
Lasers
University Science Books
- [17] Bahaa E. A. Saleh, Malvin Carl Teich
Fundamentals of Photonics
John Wiley & Sons, Inc.
- [18] Klaus Jaenich
Funktionentheorie
Springer
- [19] M. Pinard, Y. Hadjar, and A. Heidmann
Effective mass in quantum effects of radiation pressure
Eur. Phys. J. D 7, 107 (1999)
- [20] T. Briant, P.F. Cohadon, A. Heidmann, and M. Pinard
Optomechanical characterization of acoustic modes in a mirror
Phys. Rev. A 68, 033823 (2003)
- [21] M.R. Vanner, J. Hofer, G.D. Cole & M. Aspelmeyer
Cooling-by-measurement and mechanical state tomography via pulsed optomechanics
Nature Communications 4, 2295 (2013)
- [22] G.D. Cole et. al.
Megahertz monocrystalline optomechanical resonators with minimal dissipation
2010 IEEE 23rd International Conference on Micro Electro Mechanical Systems (MEMS), 847
- [23] G.D. Cole
Cavity optomechanics with low-noise crystalline mirrors
Proc. SPIE, 845807 (2012)

- [24] Frank Natterer
The Mathematics of Computerized Tomography
Society for Industrial and Applied Mathematics
- [25] L. F. Buchmann, L. Zhang, A. Chiruvelli, and P. Meystre
Macroscopic Tunneling of a Membrane in an Optomechanical Double-Well Potential
Phys. Rev. Lett. 108, 210403 (2012)
- [26] Pavel Sekatski, Markus Aspelmeyer, and Nicolas Sangouard
Macroscopic Optomechanics from Displaced Single-Photon Entanglement
Phys. Rev. Lett. 112, 080502 (2014)
- [27] Igor Pikovski, Michael R. Vanner, Markus Aspelmeyer, M. S. Kim & Caslav Brukner
Probing Planck-scale physics with quantum optics
Nat. Phys. 8, 393 (2012)

Appendix

A Pulsed cavity optomechanics

The starting point of our treatment here is the quantum Langevin equation for the optical field (in the rotating frame). Assuming resonant drive, this becomes

$$\dot{a} = (ig_0 X_M - \frac{\kappa}{2})a + \sqrt{\kappa}a_{in}. \quad (59)$$

Since the mechanical position can by assumption be approximated as constant over the pulse duration, this equation is now decoupled from the corresponding equation for the mechanical oscillator, which can formally be written as

$$\dot{b} = ig_0 a^\dagger a \quad (60)$$

during the short interaction, where we have neglected harmonic motion and mechanical damping. Equation 59 accounts for the phase shift of the cavity field reflected of the mirror as well as cavity decay and coupling to the input field, equation 60 simply describes the momentum transfer to the mirror during the interaction with the optical pulse.

We now write

$$a(t) = \alpha(t) + \delta a(t)$$

and

$$a_{in}(t) = \alpha_{in}(t) + \delta a_{in}(t).$$

Here $\alpha(t)$ is just the expectation value of a at the time t (see also the footnote on page ..) and corresponds to the slowly varying pulse shape, while δa is the usual noise operator (and similarly for $\alpha_{in}/\delta a_{in}$). From equations 59 and 60 we arrive at the linearized equations

$$\dot{\alpha} = -\frac{\kappa}{2}\alpha + \sqrt{\kappa}\alpha_{in}$$

and

$$\dot{\delta a} = -\frac{\kappa}{2}\delta a + \sqrt{\kappa}\delta a_{in} + ig_0 X_M \alpha,$$

where we have neglected the term $igX_M \delta a$. The first equation is just the classical equation describing the evolution of a complex amplitude in a cavity, while the second term describes the noise processes including the modulation of the amplitude and phase due to the motion of the mirror. Solving these equations in the time domain yields

$$\alpha(t) = \sqrt{\kappa} \int_{-\infty}^t \alpha_{in}(t') e^{-\frac{\kappa}{2}(t-t')} \quad (61)$$

and

$$\delta a = \sqrt{\kappa} \int_{-\infty}^t dt' \delta a_{in}(t') e^{-\frac{\kappa}{2}(t-t')} + ig_0 \phi(t) X_M, \quad (62)$$

where we defined $\phi(t) := \int_{-\infty}^t dt' \alpha(t') e^{-\frac{\kappa}{2}(t-t')}$. The output field is given by

$$a_{out} = \sqrt{\kappa}a - a_{in}$$

and its phase quadrature is therefore

$$P_{out}(t) = \kappa \int_{-\infty}^t dt' P_{in}(t') e^{-\frac{\kappa}{2}(t-t')} - P_{in}(t) + 2g_0 \sqrt{\kappa} \phi(t) X_M.$$

If the phase is detected via an optical homodyne measurement as described in section 3.5 and the area under the pulse is measured, the measurement operator is given by

$$P_L = \int_{-\infty}^{\infty} dt \alpha_{LO}(t) P_{out}(t),$$

where $\alpha_{LO}(t)$ corresponds to the local oscillator pulse. Assuming coherent optical states, we can evaluate the expectation value and the variance as

$$\langle P_L \rangle = \chi' \langle X_M \rangle$$

and

$$(\Delta P_L)^2 = \chi'^2 (\Delta X_M)^2 + \left(\int dt \alpha_{LO}(t) \right)^2 (\Delta P_{in})^2.$$

Here χ' depends on the form of the pulses (note that it is defined slightly different than in the last section and is still dependent on the local oscillator amplitude), for a more detailed analysis including an optimization of α_{in} and α_{LO} to maximize χ' see [5]. Together with equation 60, which determines the momentum transfer to the mirror, we can then proceed as in the last section.

The results are exactly the same, only the coupling strength χ and the momentum transfer \bar{M} will be enhanced due to the use of a cavity.

Lebenslauf



Ausbildung

1994 – 1998	Volksschule Kirchdorf, Lustenau
1998 – 2002	AHS, Gymnasium Lustenau
2002 – 2007	HTL Rankweil Elektrotechnik und Telekommunikation Fachrichtung: Technische Informatik
2007 – 2011	Universität Wien Bachelor-Studium Physik
2007 – 2014	Universität Wien Bachelor-Studium Mathematik
2011 – 2015	Universität Wien Master-Studium Physik

Arbeitserfahrung

03.07.06 – 27.08.06	Betriebspraktikum Siemens AG Abteilung: Program and System Engineering
03.09.07 – 02.03.08	Grundwehrdienst Gebirgskampfzentrum Saalfelden

15.06.08 – 25.08.08	IT - Counselor Independent Lake Camp, Pennsylvania
02.02.09 – 27.02.09 & 06.07.09 – 24.07.09 & 10.08.09 – 18.09.09	Ferialpraktikum Julius Blum GmbH Abteilung: Informationssysteme
01.05.15 – 31.05.15	Wissenschaftlicher Projektmitarbeiter Universität Wien

Fremdsprachen

Englisch	in Wort und Schrift
Spanisch	Grundkenntnisse

Publikationen

Cooling-by-measurement and mechanical state tomography via pulsed optomechanics
M. R. Vanner, J. Hofer, G. D. Cole, and M. Aspelmeyer
[Nature Communications 4, 2295 \(2013\)](#) [[quant-ph 1211.7036](#)]